Highlights

Paleoglaciology of the central East Antarctic Ice Sheet is revealed by blue-ice sediment

We present ~100 cosmogenic ages for a blue-ice moraine at Mt. Achernar, central Transantarctic Mountains.

The Law Glacier surface experienced relatively minor fluctuations in surface elevation throughout MIS 6 and 5, and likely previous.

A lateral moraine indicates the Law Glacier surface was higher at ~9.2±0.5 ka.

Blue-ice sediments are an underutilized and dateable paleoglaciologic and paleoclimate archive

Paleoglaciology of the central East Antarctic Ice Sheet as revealed by blue-ice sediment

Kaplan, M.R.[1*], Licht, K.J.[2], Lamp, J.L.[1], Winckler, G.[1,3], Schaefer, J.M.[1,3], Graly, J.A.[4], Kassab C.M.[2], Schwartz, R.[1]

[1]Geochemistry, Lamont-Doherty Earth Observatory, Palisades, New York 10964, USA

[2]Department of Earth Sciences, IUPUI, Indianapolis, Indiana 46202, USA

[3]Department of Earth and Environmental Sciences, Columbia University, New York, New York 10027, USA

[4]Deptartment of Geography and Environmental Science, Northumbria University, Newcastle-Upon-Tyne, NE1 8ST, UK

*E-mail: mkaplan@ldeo.columbia.edu

*Corresponding author: mkaplan@ldeo.columbia.edu

Keywords: cosmogenic dating; Law Glacier; Holocene; Antarctica; paleoclimate, Pleistocene; deglaciation

Abstract

We present ~100 cosmogenic surface exposure ages, including 75 new analyses, for a blue-ice moraine complex at Mt. Achernar, head of Law Glacier, in the central Transantarctic Mountains. The ^{10}Be-^{3}He-^{26}Al ages along with previously-published boron concentrations chronicle past behavior of the East Antarctic Ice Sheet (EAIS) along the edge of the polar plateau since the sediments started to accumulate, around 0.5-1 Ma. Sediments analyzed for ^{10}Be from the Law Glacier surface record <100 years of exposure, indicating they likely have negligible inheritance when first exposed. The Law Glacier surface experienced relatively minor fluctuations in surface elevation throughout MIS 6 and 5, and likely during prior periods, as geomorphic features are intact and exposure ages are coherent on the moraine, ranging from ~210 to ~86 ka; respective means for MIS 5 sediments in two different areas are 106±9.1 ka [n=4 ages] and 106±5.1 ka [n=6]. Although we infer the Law Glacier has been relatively close to its current configuration generally since 0.5-1 Ma, disturbances to Achernar blue-ice moraine architecture seem apparent at times especially prior to the last two glacial cycles. The largest observed disturbance occurred when the nearby Lewis Cliffs Ice Tongue expanded either near, or much earlier than, 500-400 ka. A minimum ice thickness increase of 30 m is associated with the ~20 ka blue-ice ridges, and a lateral moraine indicates the Law Glacier surface was ~40-50 m higher at ~9.2±0.5 ka. Our findings support that lateral accretion over time formed the Mt. Achernar blue-ice moraine sequence, and by implication, other analogue Antarctic deposits. We interpret blue-ice moraines as representing, at times, relatively constant outlet glacier conditions and concur with prior studies that they reflect near-equilibrium forms. Blue-ice sediments are an underutilized and dateable paleoglaciologic and paleoclimate archive in Antarctica, including for former ice surface dynamics and possibly as a repository of old ice during periods such as MIS 5 and prior.

1. Introduction

In paleoglaciology, former ice surfaces and their dynamics can be difficult to reconstruct as evidence is not typically left behind. This is especially true for past ice sheet interiors, including for those that still exist in Antarctica. In particular, observations of former ice sheet surfaces are not common prior to the last local glacial maximum (LGM), including in Antarctica. Blue ice ablation zones and their moraines are common throughout the Antarctic continental interior, and provide a unique means to reconstruct the surfaces of former ice sheets, including prior to the LGM (Bintanja, 1999). The primary reason is that their sediment accumulations overlie ice that is adjacent to and linked into active glacier flow (Whillans and Cassidy, 1983; Cassidy et al., 1992; Bintanja, 1999; Sinisalo and Moore, 2010).

Reconstructing past ice surface elevations is important for multiple reasons. First, we can use such evidence to document the relative stability or instability of the interior of the EAIS and other sectors of Antarctica, including during past warm periods. Second, blue-ice sediment and ice arrive from below the surface (Whillans and Cassidy, 1983; Chinn, 1991, 1994; Cassidy et al., 1992; Corti et al. 2008; Sinisalo and Moore, 2010; Palmer et al., 2012). Hence, their study improves understanding of subglacial, englacial, and supraglacial processes, as well as underlying geology that cannot be observed (Fogwill et al., 2012; Palmer et al., 2012; Ackert et al., 2013; Campbell et al., 2013; Hein et al., 2016; Westoby et al., 2016; Winter et al., 2016; Bader et al., 2017; Graly et al., 2018a,b, 2020;). Third, observations of past surfaces and outlet glacier behavior provide test beds for model experiments (Pattyn, 2010; Whitehouse et al., 2012; Golledge et al., 2013; DeConto and Pollard, 2016), including the sensitivity of different sectors of Antarctica to past warm periods. Last, age information on past surfaces may reveal sites where old ice is preserved (Higgins et al., 2015).

Detailed study of blue-ice sediments is required to understand better these features as important paleoglaciologic and paleoclimate archives. Blue-ice areas typically occur under compressive glaciological regimes where rates of sublimation and wind scouring exceed accumulation. Studies in West Antarctica show that blue-ice regions offer a dateable archive of former ice sheet behavior over the million year timescale (Fogwill et al., 2012; Hein et al., 2016; Woodward et al. 2022). In the Transantarctic Mountains (TAM) blue-ice areas also provide repositories of old ice (e.g., Higgens et al., 2015), because compressive stresses related to flow around the Transantarctic Mountains and sublimation rates bring subglacial and englacial ice towards the surface from lower, older sections of the ice sheets (Whillans and Cassidy, 1983; Corti et al., 2008).

Here, we provide ^{10}Be-^{3}He-^{26}Al cosmogenic surface exposure ages near Mt. Achernar in the central TAM and synthesize all chronologic data with prior efforts in the area (Figs, 1, 2). We use the findings to answer questions concerning the timing, amount, and stability of former ice surface changes at the head of the Law Glacier (Fig. 1) at the edge of the polar plateau, where ice converges into the central TAM. Model output shows that this sector of the EAIS may be relatively insensitive to past climate changes including warm periods (e.g., DeConto and Pollard, 2016). The data allow us to evaluate whether such simulations are consistent with observations, specifically those documenting the magnitude of changes if the central EAIS has been relatively stable.

2. Background

2.1. Mt. Achernar setting

The Mt. Achernar blue-ice moraine complex begins approximately 20 km downstream of the EAIS plateau. The blue-ice area exists at the head of Law Glacier, which is between the Queen

Alexandra and Queen Elizabeth Ranges. Topographic steering into a lee-side embayment (Fig. 1) downstream of Mt. Achernar (2691 m) traps upward flowing ice in a blue-ice area, which subsequently sublimates. Near the active Law Glacier ice/moraine edge (Fig. 3) subsurface-derived debris bands are emerging parallel/subparallel to the margin, and document how en- and subglacial sediment is added to the moraine (Kassab et al., 2019).

The Achernar blue-ice moraine is ∼100 km^2 and extends >5 km from the active Law Glacier towards the Lewis Cliffs Ice Tongue and other unnamed glaciers that flow more or less northward in the opposite direction (Fig. 1). Located around an elevation of 1700-1900 m, the majority of the moraine complex is dominated by a series of 1-12 m high ridges and troughs that run subparallel to the main flow direction of Law Glacier (Bader et al., 2017). Ridge orientation commonly mimics the shape of the active main trunk of Law Glacier (Fig. 1). Some ridges exhibit laterally continuous visible bands and till of sandstone, dolerite, or mixed lithologies that impart a generally consistent color (Fig. 4), which often provides a strategy for sampling. On sunny or relatively warm days with air temperatures still below freezing, we observed surface melting associated with dark-colored debris, especially near the boundary between the moraine and the clean ice of Law Glacier. Although seemingly minor in terms of quantity, we assume such melting may have important geomorphological effects (Graly et al., 2018b) (Fig. 3).

2.1.1. Prior studies at Mt. Achernar

Early studies of the Mt. Achernar area, including the Lewis Cliffs Ice Tongue and Walcott Névé, were conducted due to the site’s usefulness for meteorite collection (e.g., Faure et al. 1992; Cassidy et al., 1992; Hagen, 1995). Scarrow et al. (2014) studied soil chronosequences and patterns of moraine development in this arid setting and inferred that through time material is added so as to thicken progressively the soil from its base, which was documented in later as studies as well (Bader et al., 2017; Graly et al., 2018b). Near the Lewis Cliffs Ice Tongue, Sun et al. (2015) focused on the geochemistry of salts emerging from subglacial water, and argued for a sustained cold polar environment for millions of years.

Bader et al. (2017) presented geomorphic, sedimentologic, and till composition and provenance findings including pebble lithology and detrital zircon geochronology, for the Mt. Achernar moraine complex. They defined 5 zones of the moraine sequence – which we follow in this study – based on color bands and distinct differences in geomorphology; Bader et al (2017) also found the zones coincided with the relative weathering of sediments and their provenance characteristics. Briefly, Zone 1 tends to be hummocky with pronounced pond-like depressions separated by ridges (Fig. 3). The ridges and depressions exhibit in places a weak alignment that is oriented more or less at an oblique angle to the ice margin (Figs. 1D, 3). Sediments are grey or dark grey. Zone 2 is distinguished by relatively low relief with small ridges far apart (Fig. 4). Zones 3 & 4 contain well-defined continuous parallel/sub-parallel ridges and troughs (Fig. 4). Zone 4 contains sediments that are pale yellow or light-yellowish brown characteristic of weathering of sandstones, or red varnish that is associated with weathering of the Ferrar Dolerite (Mercer, 1968). Zone 5 sediment exhibits extensive red varnish and consists of parallel/sub-parallel ridges sourced in part from an unnamed northward flowing glacier. In Zone 5, two reported ^{3}He exposure ages are recalculated from Kaplan et al. (2017), and the boron data are from Graly et al. (2018a).

In the downglacier (northeast) part of the area studied, referred to as the tail, a prominent moraine ridge exhibits characteristics similar to Zone 1 (Bader et al., 2017) (Figs. 2, 5, 6). Past the moraine ridge (i.e., farther from Law Glacier) exists a snow-covered gap (<20 m wide) and then topographic moraine ridges/troughs. In places, the ridges exhibit a change in orientation so that they are oblique to the innermost moraine ridge (Figs. 1D, 2). On the other side of the snow-covered gap, sediments are pale yellow or light yellowish brown or dark red (Ferrar Dolerite) similar to in Zone 4 along the main transect; hence, just based on moraine description we conclude the gap represents a significant temporal discontinuity (Bader et al., 2017; Graly et al., 2018a).

Bader et al. (2017) also described facets and striations on up to 30% of the cobble clasts indicating an active subglacial origin, and concluded that blue-ice sediments contain a valuable record of underlying unexposed bedrock geology that cannot be directly observed. Given there is no exposed bedrock upstream of Mt. Achernar, the moraine sediment is subglacially or englacially derived with mostly local but also some non-local components (Bader et al., 2017), except for meteorites (Cassidy et al, 1992). Over the time interval represented by the moraine complex, Bader et al. (2017) inferred former ice surface changes of <40 m and relatively stable past ice sheet configurations, in part based on the geomorphology and compositional and provenance studies of glacial till and pebbles.

The first direct chronologies for the Mt. Achernar moraine (Hagen, 1995; Kaplan et al., 2017) established that the site contains sediments exposed at the surface since before the global LGM, during Marine Isotope Stage 2 (MIS 2). Bader et al. (2017) and Kaplan et al (2017) inferred the East Antarctic polar plateau has been relatively stable for at least 200 kyr. Graly et al. (2018a) analyzed salt concentrations and speciation in the top horizons of Mt. Achernar sediments. They found the concentration of boron-containing salts are highly correlated to exposure ages of nearby boulders from the same moraine ($R^2 > 0.99$) and inferred that low vapor pressure at cold temperatures and extreme aridity limit mobility of such salt species within the soil column, and major melt could not have occurred during the time the moraine existed. By calibrating boron concentrations in till soils to the first set of cosmogenic nuclide ages available from nearby boulders, Graly et al. (2018a) documented that boron concentration provides a sediment exposure age, which is used in this study.

Most recent studies at Mt. Achernar provided insights into regional subglacial and englacial processes, and general blue-ice moraine sediment formation and soil chemistry. Kassab et al. (2020) integrated ground-penetrating radar (GPR, 100 and 25 MHz) data with GPS measured ice velocity and published surface exposure ages (Kaplan et al, 2017; Graly et al., 2018a). GPR transects (100 and 25 MHz) both perpendicular and parallel to moraine ridges revealed alternating relatively clean ice and horizons where englacial debris bands dip steeply towards the surface. Kassab et al. (2020) suggested sediment generally moves upward associated with debris bands (and along shear planes?), but in certain locations there are more complicated subsurface structures. Kassab et al. (2020) also documented that the entire moraine is underlain by >150 m glacier ice, with varying amounts of debris in places including in the englacial bands. Along with Graly et al. (2018b), they estimated a maximum elapsed time of ~100-250 kyr from subglacial entrainment to transport and debris reaching the surface. Kassab et al. (2020) proposed a model to explain the formation of blue-ice moraine sequences whereby debris accretes laterally to form new moraine. They also inferred englacial sediments may continue to accumulate at the base of the already-existing moraine, agreeing with the earlier study of Scarrow et al. (2014). Using oxygen isotopes, including those from a shallow core, Graly et al. (2018b) documented that glacier ice flowing upward into the Achernar moraine system was sourced from the EAIS plateau (Fig. 1), and inferred ice and sediment entrainment in an open system under warm-based basal conditions. Graly et al. (2018b) estimated a minimum age of MIS 6 for the ice underlying and feeding the Achernar blue-ice moraine, and that ice within the current Law Glacier was slightly younger and originated during MIS 5. Last, prior papers argued that the lateral continuity of the ridges and troughs, specifically those with distinct lithologies (Figs. 2, 4), exposure age progression, and general geochemistry and till provenance signify relative stability of the moraine surface (e.g., Bader et al., 2017; Kaplan et al., 2017; Graly et al., 2018a,b, 2020).

3. Methods

We conducted field work at Mt. Achernar during the 2011 and 2015/16 austral summers, either from a nearby base camp ~6 to 20 km from the moraine sampling sites, or by several 1-day trips by helicopter from the larger CTAM (central TAM) camp. Samples for cosmogenic exposure analyses were collected in three parts of the moraine complex: 1) near and along the main part of the moraine sequence. A main transect, as indicated by the dashed-white line in Figure 2, is where the majority of samples were collected, and was largely the focus of earlier studies by our group; 2) in the downglacier (southwest) part of the study area, in an area informally referred to as the tail (Figs. 2, 5); 3) along a lateral moraine that runs along the headwall of Mt. Achernar (Figs. 4, 6).

We collected quartz-bearing sandstones and pyroxene-bearing dolerites for ^{10}Be-^{26}Al and ^{3}He, respectively. We sampled mainly boulders (> 25 cm high), but also cobbles as noted in the figures and tables. We preferentially selected boulders away from depressions (e.g., polygon boundaries) in areas where periglacial processes were apparent. Samples were taken from the upper 1-3 cm of the boulder, in the most stable-looking, horizontal/flat portion (and if possible as close to the center as possible) of the top surface. Samples were collected with hammer and chisel. A compass and clinometer were used to measure the azimuthal elevations of the surrounding landscape to account for shielding, although it was negligible in almost all cases except for the four lateral moraine samples (~1-1.5% difference in exposure age).

We used a handheld GPS (WGS 84) for all sample latitudes and longitudes. For sample elevations, we used a Trimble GPS system (EGM96), except for 9 sandstones (^{10}Be-^{26}Al) and 4 dolerites (^{3}He) as noted in Table 1. Differential processing used continuous data from a permanent base station set up on a bedrock surface that was 8 km (tail) to 20 km (lateral moraine on Fig. 2) away. For latitude and longitude, we checked all handheld GPS measurements against post-processed differential-based analyses where available, and as expected they are indistinguishable at the scale of all the figures. For elevation, we assume uncertainties are <1 m if differentially based. Comparison of handheld GPS data with differential-based elevations for 104 sites, in which both are available, yields an average offset of +9.1±4.1 m, excluding one sample that was +47.8 m higher. Except for two samples, the handheld GPS always gave higher elevations. Four samples on one particular moraine ridge were only measured with a handheld GPS, and as noted below in the Results their recorded elevations may be ~10 m too high relative to EGM96 orthometric heights; if correct, this would cause these 4 exposure ages to be <1% too low.

Processing for ^{10}Be preparation and analyses followed standard procedures at the Lamont Cosmogenic Nuclide Laboratory (Schaefer et al., 2009; Kaplan et al. 2017). A custom-made ^{9}Be carrier allows measurement of samples with extremely low concentrations, 1000-2000 ^{10}Be atoms/g (Table 1). Almost all samples were measured at the Center for Accelerator Mass Spectrometry at Lawrence Livermore National Lab, except for nine samples associated with blank BLK2017May10 (Table 1), which were analyzed at PRIME Lab. All ^{26}Al analyses in this manuscript are from Kaplan et al. (2017), although they were recalculated with up-to-date systematics.

All reported exposure ages were calculated using Version 3 of the online cosmogenic exposure age calculator hosted by the University of Washington (https://hess.ess.washington.edu)

(Balco et al., 2008), including ages updated from Kaplan et al. (2017) and Hagen (1995). ^{10}Be and ^{26}Al ages are presented based on the production rate calibration dataset from Kaplan et al. (2011) for ~50°S in southern South America, which is the closest geographically to Antarctica. This rate is statistically indistinguishable from the other middle latitude Southern Hemisphere ^{10}Be production rate calibration, derived in the Southern Alps of New Zealand at ~43°S (Putnam et al., 2010). We present results using three latitude and elevation-dependent production rate scaling methods (St, Lm, LSDn) (Table 3), although for the sake of discussion we show and discuss the time dependent version of Lal (1991)/Stone (2000) (Lm) except where noted.

A recent study by Balter et al. (2020) presented evidence that (at least) at high elevation Antarctic sites and for samples exposed continuously for $>10^6$ years, the production rate calibration dataset of Borchers et al. (2016) and the LSDn scaling method (Lifton et al., 2014) are perhaps most appropriate for calculating exposure ages. In the Discussion, we also provide ages derived with the rate in Borchers et al. (2016) and LSDn scaling where it may slightly affect our inferences, specifically for the oldest exposure ages. Although we present and discuss ages using the Lm (Lal, 1991; Stone, 2000), Table 2 shows differences if LSDn (Lifton et al., 2014) is used instead. For almost all cosmogenic ages, LSDn scaling affords ~10% younger ages than Lm, except for samples exposed for ~1000-2000 years (13-14% younger) and for the last 100 years (0 to 5% older). If the ^{10}Be production rate dataset in Borchers et al (2016) is used instead of the middle latitude Southern Hemisphere dataset (Kaplan et al. 2011; *cf.*, Putnam et al., 2010), the exposure ages become 5% and 2% lower using the Lm and LSDn scaling methods respectively.

Processing of pyroxene separates and ^{3}He analyses followed standard procedures at the Lamont Cosmogenic Nuclide Laboratory (Bromley et al., 2014; Eaves et al., 2015, 2016; Kaplan et al. 2017). Abundance and isotopic analyses are performed with a MAP215-50 noble gas mass spectrometer. Analyses are against either a known volume of a Yellowstone helium standard (MM), or air, as noted in Table 2. As in the case of ^{10}Be and ^{26}Al, we used Version 3 of the online calculator at https://hess.ess.washington.edu (Balco et al., 2008) to calculate new, and recalculate previously published (e.g., Kaplan et al., 2017), ^{3}He exposure ages. Analogous to ^{10}Be and ^{26}Al, we present results from three scaling methods (Table 3), although we show and discuss ages derived with Lm, the time-dependent version of Lal (1991)/Stone (2000), except where noted. Eaves et al. (2015) examined the cosmogenic $^{3}He_{px}$ production rate in the south-west Pacific (39°S) and found it indistinguishable from the default production rate calibration dataset of Borchers et al. (2016).

^{3}He concentrations and resulting exposure ages presented here are not corrected for noncosmogenic (nucleogenic and inherited mantle-derived) ^{3}He in the samples. Unlike in Kaplan et al. (2017), we do not report ^{3}He ages with and without subtracting an inferred inherited or nucleogenic fraction. Kaplan et al. (2017) and Balco (2020) suggested noncosmogenic concentrations roughly in the mid-10^{6} atoms/g range consistent with prior estimates (e.g., Ackert, 2000). As most of the ^{3}He exposure ages presented here contain 10^{7}-10^{8} atoms/g (i.e., >10 ka, Tables 2 and 4), the effect is not significant in terms of our findings and conclusions. A future manuscript will discuss such ^{3}He corrections at Mt. Achernar.

All cosmogenic nuclide exposure ages reported in Tables 3 and 4 assume no erosion. As Antarctica has some of the lowest erosion rates on Earth (Schäfer et al., 1999), for most samples we assume erosion is insignificant. In fact, some of the boulders are still striated (e.g., <10 ka). Nonetheless, we point out that if we assume an erosion rate of ~10 cm Ma^{-1}, the ~500 ka ages (oldest) increase by ~5%. Also, we do not correct for snow cover on the boulders. We point out that by definition blue-ice areas contain generally little or no snow (Bintanja, 1999). Although some snow may accumulate in small depressions, we avoided sampling in such spots. Hagen (1995) noted that their one prominent young exposure age outlier of ~15 ka could be explained by the fact it was collected from a depression with snow (Fig. 2), as mentioned in Kaplan et al. (2017).

4. Results

For the ease of presentation, below we describe results separately for three parts of the Mt. Achernar area: the main moraine sequence, the tail area, and the lateral moraine along the headwall of Mt. Achernar (labeled on Fig. 2). In addition, we refer to Zones 1 to 5, as first described in Bader et al. (2017) and elaborated on in Kassab et al. (2020) and reviewed above in Section 2.2. Furthermore, Graly et al. (2018a) sampled several moraines for boron concentrations (Fig. 1c) that were not dated in this study with ^{10}Be-^{3}He-^{26}Al. The calibrated boron approach thus adds to the exposure chronology of the entire moraine system (Fig. 7), and ages are mentioned here in Results where pertinent.

4.1. Main part of moraine sequence (Figs. 2-4, 6-7)

Most measured samples come from boulders (and 3 cobbles) located close to a transect that was the focus of prior studies, shown by the white-dashed line in Figure 2. In Zone 1, we analyzed three samples associated with active, relatively clean Law Glacier ice, near the contact with the moraine (Fig. 3). A boulder yields a ^{10}Be exposure age of 79 ±5 yrs, and two cobble-sized samples 52±4 and 76±8 yrs; thus samples near the Law margin record <100 years of apparent exposure. Two nearby samples around the ice/moraine contact but on the moraine have ^{10}Be ages ~600-1000 years (MAR-15-110, -111); these results are consistent with two ^{10}Be ages just to the east (Fig. 2B; MAR-15-139, -142h), near a small embayment in the moraine, which give essentially identical ages, ~800-700 years for apparent exposure. Inward, along Zone 1 sediment (Figs. 3,7), exposure ages steadily increase to around 10 ka. Three dolerites yield apparent ^{3}He ages of ~7 ka and ~14 ka (MAR-11-01,-02, -112c), the first two of which were previously published. As Kaplan et al. (2017) noted, these three apparent exposure ages may record primarily non-cosmogenic ^{3}He concentrations, with some cosmogenic component given their presence in Zone 1. Given the large uncertainty for MAR-15-61 (>20%), its age of 2.8±0.7 ka is not used (Table 1).

In Zone 2, exposure ages remain around 14-10 ka, with one discordant ^{26}Al age slightly older. In Zone 3, ages increase to ~55 ka (Figs. 4,7). This includes four coherent ages dating to 19.3 ±0.8 (excluding one outlier of ~5.9 ka), and a cluster between ~55 and 35 ka (excluding one outlier of ~14.3 ka). We note at least six ridges remain undated in Zone 3.

In Zone 4, we sampled ~5-6 ridges. Exposure ages begin around 100 ka and steadily increase (Figs. 2,7). Four coherent ages date to 106±5.1 ka; in addition, two younger ages on different samples are 57.8±3.0 and 39.9±1.7 ka, respectively, with the lowest age on a cobble-size rock. Slightly farther away from the Law Glacier to the southeast, two ages are 135.2 ±2.2 and 120.0±2.5 and one nearby younger age is 86.1±1.3. A cluster of ages ranges from ~213 to 177 ka, along with one younger age of 73.7±4.3 ka. The oldest ^{10}Be-^{26}Al ages towards the back of Zone 4 are ~530-450 ka. The oldest ^{3}He age is ~380 ka. One cobble-size sample near the ~500 ka boulder dates to ~370 ka. The boron analyses are consistent with ~500 kyr, or possibly 500-400 kyr, of exposure (Fig. 7; Graly et al., 2018a). Close to the Lewis Cliffs Ice Tongue, exposure ages reverse and become younger. Exposure ages reported in Hagen (1995) are consistent with the new data (Fig. 2). We note that sample elevations for MAR-15-123 to 126 were measured only with a handheld GPS, which tended to be ~10 to 9 m higher than differential-based elevations; if the elevations are too high by ~10 m, the resulting exposure age would be typically ≤1% too low, which is within age uncertainties. In summary, we obtained a large number of ages around 210-177 ka and 135-86 ka.

In Zone 5, which is farthest from the Law Glacier (Fig. 1C), two ^{3}He ages are 109±3 ka (MAR-11-48) and 316±7 ka (MAR-11-52). The ~109 ka boulder is closer to the boundary of sediments associated with the Lewis Cliffs Ice tongue (Fig. 2A), it is greyer in color and located near material with less varnish, and it appears to be surrounded by depressions on the order of a few meters that we assume are caused by periglacial processes. In contrast, the ~316 ka sample is farther into Zone 5 (Fig. 2A) and surrounded by sediments with extensive red varnish. Closer to the unnamed glacier, slightly farther south, Graly et al. (2018a) obtained boron exposure ages of ~1 Ma and ~680 ka.

For the entire exposure age distribution in the main sampling area, an exponential relation can describe the increase in ^{10}Be-^{3}He-^{26}Al-Boron ages with distance from relatively clean Law Glacier ice (Fig. 7), with an R^2 >0.7. For surface sediments exposed <50 kyr, or up to ~2200-2000 m from Law ice, a linear relation also can be used to represent exposure age versus distance, with an R^2 of ~0.8 (^{10}Be) or ~0.6 (^{3}He). That is, a break in slope, or a notable change in the samples' exposure age versus their distance from Law Glacier occurs around 50 ka or at least prior to the last glacial cycle.

4.2. Tail area (Fig. 5)

In the downglacier sector of Mt. Achernar, we analyzed samples from recently emerged debris along the edge of the Law Glacier, from the prominent grey-colored, unoxidized moraine positioned east of the ice-contact area, and also from the light-yellowish brown and red till located on the other side (east) of the prominent snow gap (Figs. 2, 5, 6). Closest to relatively clean Law ice is the youngest exposure age (320 years). A short distance away (~10 m) from Law Glacier and slightly higher (about +4 m), ages increase to ~2700-1100 yrs, similar to those observed in the main area (Figs. 2, 3). The prominent right lateral ice-cored moraine of gray till is continuous for several kilometers and eventually dissipates downstream. On this moraine, we obtained a relatively wide age distribution from ~1 ka to 18 ka. A boulder and cobble (MAR-15-132, -133) provided ages of ~740 years and ~1.7 ka, respectively. Close to these two ages of <2 ka, and still on the grey unoxidized moraine, is a boulder age of 15.1 ±0.2 ka, and at the end of the tail is another boulder age of 17.8 ±0.3 ka. The two boulder ages ~15-18 ka are located in the last ~1,200 m before the tail dissipates, and they do not appear to have a relation with distance from the Law ice edge; the ~15.1 ka boulder is located slightly closer to the Law margin compared with the 1.7 ka sample.

East of the grey moraine by ~50 m, samples were collected from the light-yellowish brown and red oxidized till. Here moraine ridges are oblique to the gray moraine and six ^{10}Be-^{3}He dates offer a coherent age cluster of 103.1±8.9 ka, or 105.9±5.1 ka excluding an age of 85.8±1.7 ka, and an obvious outlier of ~18.6 ka (Fig. 5). A second set of three ^{3}He ages slightly farther to the southeast (MAR-11-41 to 43) date to 160-110 ka. There is a difference of about 60-80 kyr – close to a full glacial cycle – between the light-yellowish brown/red oxidized and the unoxidized moraine areas. The unoxided and oxided sediments are at similar elevations, with the latter (i.e., lateral moraine) being slightly higher by ~5-10 m. The light-yellowish brown and red oxidized sector is about the same elevation as the modern ice surface, ~1750-1740 m (Fig. 5).

4.3 Lateral moraine along headwall of Mt. Achernar.

Four cobble-sized samples were ^{10}Be dated along a lateral moraine that runs along the west-side headwall that bounds the Achernar moraine complex (Figs. 2,3). The ages form a relatively coherent distribution with a mean age of 9.2±0.5 ka. The moraine is approximately 40-50 m above the current clean ice margin (Fig. 6D-F), and is oriented more or less in the direction of flow into the lee side embayment and towards the Mt. Achernar moraine (Kassab et al., 2020), and oblique to the flow of the trunk of Law Glacier (Fig. 1). The moraine slopes about 20m/km southeastward towards the middle of the moraine complex and appears to end in inner Zone 4, just past the 100 ka ridges of the main area. There is a trimline that is higher than the lateral moraine, by <20m and <10m close to Law Glacier and adjacent to inner Zone 4, respectively. This trimline remains undated and is discussed further in Section 5.3.

4.4 Boulders vs cobbles

We sampled cobble-sized sediments to compare their exposure ages with those of boulders. By the ice/moraine contact, one boulder and two cobbles have similar apparent exposure ages (~80-50 yrs). In the back of Zone 4, one cobble-size sample (MAR-15-113c) was obtained near the ~500 ka boulder and is notably younger (370±7 ka). For comparison, the nearby boron concentration is consistent with 500-400 kyr of exposure (Fig. 7; Graly et al., 2018a). In the tail area, the cobble-sized sample (MAR-15-88) has a ^{10}Be result (~1.1 ka) consistent with other nearby boulders and cobbles; in addition, it is slightly farther (~10-20 m) away from the sample exposed for less time, ~320 yrs, and present clean ice edge (Figs. 5, 6).

4.5 ^{26}Al and ^{10}Be comparison

Kaplan et al. (2017) reported ten ^{26}Al/^{10}Be pairs, with one sample (MAR-11-14) measured twice (Tables 2, 4) as well as 6 pairs previously from Hagen (1995). In general, the fifteen samples do not contain substantial evidence for complex histories of burial and re-exposure (Fig. 8). Three samples (~20%) plot just below the constant exposure line at 1σ (but not at 2σ). Taken at face value, these three samples may contain evidence of some burial history. In more detail: 1) MAR-11-33 gives a ^{10}Be age of 36.4 ±0.5 ka, which is also one the younger ages of the distribution in this part of the moraine (excluding an obvious outlier of ~12.9 ka), perhaps related to its relatively short burial history; 2) The oldest sample measured, MAR-11-14, has discordant ^{10}Be-^{26}Al ages (529±7, 439±10, a result reproduced in the duplicate sample (532±7, 455±11 ka). Two possible analyses of MAR-11-14 (Fig. 8) include the following. (i) The sample plots along a line of continuous exposure but with erosion causing concentrations close to saturation. Sandstones exposed for 10^5 years may start to disintegrate, a finding noted in earlier studies (e.g., Denton et al., 1993). (ii) Alternatively, MAR-11-14 also may exhibit some history of burial, or both erosion and burial have produced the sample concentrations. The oldest sample in Hagen (1995) may also have a similar history as MAR-11-14, with either some erosion or burial perhaps causing slightly discordant ages (at 1σ, but not 2σ).

5. Discussion

5.1 Chronology

The Mt. Achernar area preserves one of the best-dated and coherent blue-ice moraine sequences in East Antarctica. Statistically significant relations between distance and ^{10}Be-^{26}Al-^{3}He-Boron exposure ages (Fig. 7) document a net increase in exposed time from the Law Glacier margin. An exponential increase in exposure age versus distance from Law Glacier, especially >50 ka (Fig. 7A), implies shorter spacing between the older ridges (Kassab et al., 2020), or an amount of original moraine morphology is less well-preserved and there are temporal gaps, or both. For deposits <50 ka, exposure age is linearly related to distance (up to 2200 m from Law ice); r^2 for ^{10}Be is ~0.8.

For the oldest sectors, we infer the following based on a synthesis of new and previously published findings. First, farthest from the Law Glacier, sediments have been exposed close to 500 ka, and perhaps as long as ~1 Ma (Graly et al., 2018a). The two oldest boron-exposure ages farthest from the Law Glacier in Zone 5 (southwestern sector) are ~670 ka and ~1000 ka (Figs. 2,7). We assume undated ridges in the southwestern and southeastern sectors of Mt. Achernar area (Figs. 1, 2) are between ~500 ka and ~ 1 Ma. For the oldest Law Glacier-derived ridges in Zone 4, four cosmogenic ages (one cobble-size) and two boron ages are in the ~500-400 ka range. The oldest ^{10}Be-^{26}Al sample (MAR-11-14), around 500 ka, also may be a slight underestimate for its exposure duration as the discordance between the ^{26}Al and ^{10}Be ages hints that some degree of erosion and/or burial modified the concentrations (Fig. 8). Our inference is consistent with Sun et al. (2015), who concluded that relatively cold dry conditions have existed since the Miocene based on the geochemistry of salts that are of subglacial origin near the Lewis Cliffs Ice Tongue margin. Second, the Lewis Cliffs Ice Tongue expanded into the Achernar moraine system, before or close to ~500 ka, given the cross-cutting relation with the dated Law moraine (yellow dashed line on Fig. 2A).

The last ~200,000 years of the moraine history is well documented by a large number of exposure ages from samples collected on quasi-continuous and often well-defined moraine ridges (Fig. 2). Sediments exposed since MIS 6 and 5 are found in both the main transect and the tail areas. Two ages are 135.2±2.2 and 120.0±2.5, four coherent ages provide a mean of 106±9.1 ka (Section 4.1), and six ages cluster around 103.1±8.9 ka (Section 4.2); a younger age of ~86 ka was found in both the main transect and tail areas, respectively. Notably, two samples associated with the ~100 ka deposits, 57.8±3.0 and 39.9±1.7 ka (on a cobble-size sample), overlap in age with the younger moraine ridges dated from ~55 to 35 ka. Perhaps these rocks came to the surface later (see Section 5.4), associated with only localized moraine disturbance around the sample location. The prominent lateral moraine is 9.2 ±0.5 ka, which overlaps with the chronology in the back of Zone 1 (Figs. 3, 7) and dates an early Holocene high in the Law Glacier surface.

The youngest exposure ages obtained from the Law Glacier surface are <100 years for two cobble-sized samples and a boulder (Fig. 3). These three ^{10}Be ages, as well as other analyzed samples near the tail (Fig. 5), indicate that when debris reaches the surface, it is likely to be essentially free of *in situ* cosmogenic nuclides. As nuclide production occurs even before the material reaches the surface, ages <100 years or a few centuries indicate minimal inheritance and relative rapid upward movement (to be discussed in a future paper). Moreover, the general concordance between ^{10}Be, ^{3}He, ^{26}Al and boron exposure ages and their progression with distance from Law Glacier, also indicates there is minimal inheritance in the moraine sediments, at least within the uncertainties of the three chronometers and dating of the ridges (Table 2); ~15% of the samples may have some degree of complex history, based on non-concordance with the constant exposure trajectory of ^{26}Al/^{10}Be when 1σ is considered (Fig. 8). At Mt. Achernar, a lack of pre-exposure of surface material is consistent with prior studies that concluded sediment is commonly sub-glacially derived, given it is faceted and striated (Bader et al., 2017; Graly et al., 2018b).

Several ages on cobble-size samples allows for comparison with larger boulder ages. We do not find a consistent offset. Cobbles are slightly younger in some instances, although in others they are the same (near modern Law ice) or older (tail). In the back of Zone 4, a cobble next to a boulder is distinctly younger (500 ka versus 370 ka); although the younger cobble-size sample overlaps with another nearby boulder age of ~382 ka (MAR-11-13), the older sample is consistent with boron exposure ages of 500-400 kyr (Fig. 7; Graly et al., 2018a). Whether the cobble is younger because it is smaller, reached the surface later, or was affected more by periglacial processes compared with the larger boulder is unknown. Cobble-size samples were ≤5 cm thick from the side facing upwards (apparent) to its bottom (Table 1), and we processed the width of the sample, which should reduce effects of possible rotation; for the other two axes, cobble-size samples were typically ≤5 cm 'wide,' except MAR-15-59 which is <10 cm wide. The thickness correction does not take into account, though, if the cobbles have complex histories of exposure and burial. Although as mentioned above, cobbles that were (at least) recently exposed appear to lack inherited concentrations. Additional data, including perhaps other nuclides with different half-lives, are needed to decipher the precise age of the oldest deposits, and also whether the cobble-sized materials typically afford younger ages than boulders.

A large span of the history represented in the Mt. Achernar moraine system still remains unknown. Only a handful of ridges were sampled even in the main transect (Figs. 2-5). Most of the ridges that are between ~300 ka and ~20 ka in age remain undated (Fig. 2). Between the MIS 3 (~55-35 ka) and MIS 2 (19.3 ±0.8) dated sites, there remain ~10 unanalyzed ridges. The southwestern and southeastern sectors, which may be the oldest, and most of the tail remain unsampled.

5.2. *Past central EAIS stability*

The Achernar moraine directly chronicles past Law Glacier behavior through its internal architecture, morphology, and elevations of its current surface and lateral moraine (Fig. 3). These are independent measures of either quantitative or qualitative changes in ice elevation over time. Starting with internal architecture, surface sediments exposed >10 ka (10^4-10^5 yr timescale) overlie an estimated 140-190 m of debris-rich ice; and surface sediments exposed <10 ka overlie ~220 m of relatively clean ice (Kassab et al., 2020) (Figs. 3, 9). All or most of the dated Achernar moraine thus overlies glacier ice. And, the relatively cleaner ice exposed for <10 kyr (or 20 kyr?) links into the trunk of Law Glacier. Ice and debris move upward, with the latter focused along debris bands that are connected to the topographic highs that are moraine ridges (Figs. 3,9) (Kassab et al. 2020). In this way, the Achernar site is analogous to other Antarctic blue-ice moraine sediment areas (e.g., Campbell et al., 2013; Hein et al., 2016; Akçar et al., 2020; Woodward et al. 2022).

An important consequence of the aforementioned structure below the moraines is that if, or when, the surface of Law Glacier lowers substantially it would disturb the moraine architecture, including the well-defined geomorphology and the long, mostly continuous parallel/sub-parallel ridges and troughs that contain sediments exposed for 10^4-10^5 years (Figs. 3-5). In a scenario whereby the buttressing support of Law Glacier ice is removed, it would cause surface slopes to be reversed and, eventually, drawdown of the blue-ice sediment ridges. Woodward et al. (2022) described such a scenario in the Heritage Range, West Antarctica, where thinning and a reversal of flow occurred in a blue-ice moraine setting. Previously, based on the till characteristics and provenance, Bader et al. (2017) concluded that the debris sources of the Mt. Achernar sediments were relatively constant over time, which also indicates relative stability of the central EAIS.

Our findings, as well as those in prior studies (e.g., Scarrow et al. 2014; Bader et al., 2017) raise questions including: (1) When did the preserved sediments first start to collect? (2) When and how was the Mt Achernar blue-ice moraine disturbed, in ways that are recorded in its geomorphology and chronology, which reflect major changes in paleoglaciology? On the first question, as discussed above, we infer the oldest part of the moraine (Fig. 2) is at least 500-400 ka and perhaps close to 1 Ma. Additional data are needed to evaluate further when the sediment started to collect. On the second question, we infer that an important disturbance occurred when the Lewis Cliffs Ice Tongue grew and impinged on the main area (Fig. 2A). Lewis Ice disturbed the Achernar moraine, close to or before 500-400 ka. The timing may be before or during MIS 11 (*424,000 to 374,000 years*). With one exception, the oldest exposure ages in the back of Zone 4 are around or younger than MIS 11. Moreover, we note that the 500-300 ka ages in the back of Zone 4 decrease by about 10% and lie in the ~450-300 ka range (Table 2) if the LSDn scaling method (Lifton et al., 2014) and a lower production rate are more appropriate for use in high latitudes and on older surfaces in Antarctica (Balter et al. 2020). If correct, the findings imply slightly higher central EAIS surfaces during or before MIS 11, at least associated with the Lewis Cliffs Ice Tongue. In comparison, Blackburn et al. (2020) recently inferred an MIS 11 impact to the central EAIS, specifically recession around the Wilkes Basin. Another disturbance to the Achernar moraine morphology is recorded by the age discontinuity in the tail area, as much of a glacial cycle appears missing between the grey lateral moraine and the oxidized till, which is discussed more below.

5.3. *Past Law Glacier surfaces*

At Mt. Achernar, the magnitude of glacier surface changes that disturb moraine architecture is an outstanding question. Relatively minor surface elevation changes occurred at the heads of central TAM outlet glaciers, including thinning during much of the middle-late Holocene (cf., Mercer, 1968; Denton et al., 1989; Todd et al., 2010; Bromley et al., 2012; Hall et al., 2013), as also documented here. At Mt. Achernar, disturbances to blue-ice moraine may depend on the rate as well as the magnitude of surface elevation changes, especially relative to the subglacial bedrock elevations. We infer minimal changes in the magnitude of glacier surface elevation over (at least) the time periods in which dated sediments are preserved. Surface elevational changes over the last ~500-400 kyr must have been minor enough to have left "intact" Zones 3 and 4 (10^4-10^5 yrs).

Our inferred estimates for past surface changes around the Mt. Achernar blue-ice moraine are based on several observations. First, the far-maximum possible elevational drop (thinning) from the current ice surface is ~150 m, which is depth of the underlying bedrock ridge (Kassab et al., 2020). We conclude that such a decrease has not occurred, otherwise debris would have been removed from the Mt. Achernar moraine sequence. Second, a minimum of ~50 meters of widespread ice surface elevation change is needed to disturb the moraine, following Bader et al. (2017). The right lateral moraine along the headwall of Mt. Achernar shown in Figure 6D-F indicates ~40-50 m of thickening close to the present Law Glacier at ~10-9 ka (Bader et al., 2017). We assume the right lateral moraine formed alongside the margin of a slightly expanded Law Glacier, as it flowed off the plateau along Mt. Achernar. For about 0.5-1 km distance inward the Achernar moraine appears relatively disturbed (see yellow lines on Fig. 6G), although some semblance of moraine ridges and troughs still exist (Kassab et al., 2020). Thus, the high glacier surface at ~10-9 ka and subsequent drop appears to have modified only a small area of the Achernar moraine system close to the headwall. As the lateral moraine descends (southeastward) away from Law Glacier and ends, the Mt. Achernar moraine regains a well-preserved ridge and trough form (Fig. 6G).

Above the lateral moraine, a trimline (Figs. 3, 6) exists that separates material of different relative weathering and indicates a higher ice surface before ~9.2 ka. We estimate that it is ~15-20 m and <10 m above the lateral moraine, near MAR-15-92 and -96, respectively. These may be minimum estimates given the slope and rockfall (Fig. 6 E,F). As the trimline is on a steep scree slope, we did not collect samples for exposure dating. Implications of the higher, undated trimline are as follows. First, if the trimline is older than or around ~500-400 ka, its age may reflect thickening of Law Glacier at the same time as the Lewis Cliffs Ice Tongue expanded (Section 5.1). Second, if the trimline is <500-400 ka in age, then its occurrence indicates ice surface elevations may have been higher by a minimum of ~70 m (~50 m for the lateral moraine plus ~20+ m to the trimline) near MAR-15-92 and ~10-20 m (i.e., above the blue-ice moraine) near MAR-15-96. If the trimline is <500-400 ka in age, such increased (and then decreased) ice surface changes still did not disturb more than a relatively small area (Figs. 2, 6G), and the blue-ice moraine system still remained buttressed by Law Glacier.

A third line of evidence for relatively limited surface changes associated with preserved sediments comes from the tail area, where the elevation of the oxidized sediments dated to MIS 6 and MIS 5 is the same as the present Law surface (Fig. 5), ~1750-1740 m. The grey-colored or unoxidized moraine, dated from ~18 ka to ~1 ka, is about 5-10 m higher than the present Law Glacier surface; this change, albeit possibly a minimum, did not disturb older, ≥100 ka deposits that are only ~300 m away.

Fourth, changes of ≤30 m since MIS 2 across a widespread sector of the main area of the Achernar moraine also did not disturb the older Zone 3 and 4 ridges shown in Figures 2 and 4. The precise amount of current elevational change across the moraine varies depending on where measured, which perhaps reflects localized processes or effects (Figs. 3, 7), such as sub-surface ice behavior including relative to bedrock depth. The ~20-19 ka section of the moraine is about ~20-25 m above the current Law Glacier surface, perhaps indicating higher ice input during the global LGM. From ~14 to ~10 ka, there may have been relatively less ice input into the moraine (Bader et al., 2017). Ice input then increased by ~9.2 ka, when the lateral moraine formed.

We note the net or steady rise in the moraine surface with distance from the Law Glacier, shown in Figure 7. The back of Zone 4 is about 40 meters above the present ice surface, before the topography declines back towards Lewis Cliffs Ice Tongue. We assume the increasing subglacial bedrock elevations along with the englacial flow (Kassab et al., 2020) allow sediment-moraine surface elevations to increase slightly, away from the buttressing Law Glacier. The insulation of the overlying sediment, which reduces sublimation as it thickens (Lamp and Marchant, 2017), may also allow slightly higher surfaces away from Law ice (Figs. 7,9).

5.4. Blue-ice moraine processes including formation

The chronology allows us to build upon prior studies at Mt. Achernar (Scarrow et al., 2014; Bader et al., 2017, Graly et al., 2018a,b, 2020; Kassab et al., 2020), to improve our understanding of blue-ice areas and associated processes, refine conceptual models, and to raise new questions. Any conceptual model needs to account for the increase in surface exposure age and till thickness with distance from Law Glacier, change in sediment concentration in subsurface ice, and how new sediment ridges form at the Law edge-moraine margin (Figs. 2-7, 9).

In the main moraine area, the debris concentration in the englacial ice is substantially greater below sediment surfaces exposed longer than 50 ka, compared with younger parts of the moraine (Fig. 9). Below sediment surfaces exposed >50 ka, there is a lack of distinct GPR reflections; Kassab et al. (2020) hypothesized the amount of subsurface debris becomes high enough that GPR reflections interfere with each other and no individual hyperbolic reflections are therefore observed. In association with the large ridges, especially for those exposed ~50-35 kyr, the dipping reflections appear to cluster and merge. Kassab et al (2020) inferred that underlying the innermost moraine (Fig. 3, Zones 1 and 2) the lack of reflections indicates clean ice or that with low debris concentration given the resolution (Fig. 9).

The chronology tied to the GPR-based findings lead us to infer that a significant change in englacial sediment concentration occurred around or by ~50 ka, which was caused, at least in part, by even earlier changes in basal entrainment (Fig. 9). For moraine exposed longer than 50 kyr, we infer slower subsurface ice velocity including upward movement (Fig. 9; Kassab et al., 2020), compared with that under younger parts of the moraine. Till thicknesses of ~15 cm to >1 m associated with exposure ages >20 ka (Scarrow et al., 2014; Bader et al., 2017) are consistent with slower rates of subsurface ice velocities. As till thickness increases, sublimation is reduced and eventually may be effectively shut off (Lamp and Marchant, 2017). Sublimation helps drive ice upwards (Whillans and Cassidy, 1992), hence, as its rate declines under thickening sediment 'horizontal' and upward ice velocities should decrease or essentially stop. In contrast, till thickness <10 cm are associated with the youngest Zone 1 sediments (Bader et al., 2017), where the subsurface ice is relatively clean and moraine is still forming.

The ^{10}Be-^{3}He-^{26}Al-Boron exposure ages allow us to refine an apparent sequential lateral accretion rate, as new ridges formed at the moraine-Law Glacier margin (Kassab et al., 2020). The accretion age may be similar to surface exposure age, and both may differ substantially from the ice and sediment entrainment age (Fig. 9) (Graly et al., 2018b). We confirm the apparent rate of debris accumulation and lateral growth has not been constant over time (Fig. 7B). The fastest estimated rates of lateral accretion, >60 m/kyr, are associated with a distance of ~800-400 m from the margin or roughly the ~15-5 ka exposed interval. Average rates >50 m/kyr are generally characteristic of the inner 2000 m or last ~50 kyr. For moraine exposed from ~50 ka to 1 Ma, there is a net decrease and then relatively constant and low apparent accretion rate, which is reflected in the exponential relation between ages and distance from the margin (Fig. 7A). Additional analyses are needed on ridges >50 ka to determine whether decreased apparent accretion rates reflect gaps in preservation or the moraine becoming spatially compressed, or both.

Down flow from Mt. Achernar, the tail area records a different history than the main area studied. The overall form of the tail is parallel or quasi-parallel with the current Law Glacier flow direction (Figs. 1, 2A). We infer that formation of the tail has been influenced by prevailing ice flow direction in a different manner than that of the main area (Fig. 1C,D). Furthermore, although well-developed moraine ridges exist, particularly associated with the grey unoxidized till, they are not as prominent throughout the older parts of the tail as they are in the main area (Fig. 2). Some ridges in the tail are at a different orientation and appear cross-cut by the young grey moraine. In addition, there is an age discontinuity in the tail area of ~60-80 kyr, which does not appear in the main area. For now, we speculate a change in ice thickness occurred in relation to the subglacial bed elevation, which altered the spatial pattern of debris entrainment between the tail and main transect area closer to Mt. Achernar. Perhaps a shallow subglacial bedrock ridge exists between the main area and the tail that shifted the accretion pattern as ice thickness changed, even by relatively minor amounts. However, additional geophysical (e.g., GPR) and chronological observations are needed to understand why the discontinuity exists in the downstream tail area during the last glacial cycle.

Under particular conditions, blue-ice moraines can develop towards equilibrium forms (D. Sugden personal communication). Over time, sublimation causes a progressive loss of glacier ice and thickening of surface sediments, which is documented for moraine exposed for >50 ka in the main at Mt. Achernar. Continued compressive glacier flow also may increase the concentration of debris and perhaps ridges in older parts of the blue-ice moraine (e.g., Fig. 7). Younger samples within an otherwise relatively coherent older population (Section 5.1, 'so-called outliers'), or variability in exposure ages, might be expected if sublimation caused a boulder or cobble to reach the surface long after (most of?) the moraine formed; resulting exposure age variability may be due to active subsurface debris planes. Individual samples also may be younger because localized periglacial activity caused them to move downward or rotate, and later re-emerge at the surface. Our inferences are consistent with others' conclusions elsewhere in Antarctica (e.g., Fogwill et al., 2012; Ackert et al. 2013; Hein et al., 2016; Woodward et al., 2022).

5.5. Comparison with global ice sheet changes

We display our results alongside the benthic $\delta^{18}O$ record, which allows comparisons between exposure ages and past global climate and ice sheet changes (Lisiecki and Raymo, 2005) (Fig. 10). Given that most ridges are not yet dated we highlight again, especially for older parts of the Achernar moraine sequence, inferences are tentative as only parts of its history are known. The findings imply slightly higher central EAIS surfaces during or before MIS 11, at least to cause growth of the Lewis Cliffs Ice Tongue. Moraine ridges not yet dated may reveal an MIS 4 (cf., Doughty et al., 2021) part of the sequence. As MIS 5 ages are found both in the main and tail areas, and considering the well-preserved geomorphology formed during MIS 1 (<11.8 ka), the findings imply other prior interglacial periods also might be well represented in the Mt. Achernar moraine. In fact, despite sampling only a small number of ridges in the main area and a small part of the tail, the distributions of MIS 5 ages overlap statistically, ~105-100 ka (Lm, LSDn ages are ~10% lower). Exposure ages between ~100 and 80 ka imply all MIS 5 intervals may be represented.

The time since MIS 2 is well documented, given sampling was comprehensive (Fig. 10). There are no exposure ages overlapping with the first half of Termination I, when ice receded globally (Denton et al. 2010, 2021), except for one ^{26}Al age that is high relative to its paired ^{10}Be analysis (MAR-11-22). Perhaps there was less sediment delivery during peak Termination periods, which is also consistent with the conclusion of Kassab et al. (2020) that colder global periods have higher debris concentration and entrainment. Such changes in sediment concentration may correspond to ice flow history relative to loci of entrainment, with closer sources leading to higher concentrations. However, given the lack of ridges dated, such inferences need to be tested with additional analyses. A high surface elevation around 9.5-9 ka is consistent with other interior EAIS studies that observed thick ice during the early Holocene, perhaps associated with a lag response to downstream dynamics or increased accumulation on the plateau (e.g., Hall et al., 2012).

6. Conclusions and Questions

Blue-ice moraine sediments at Mt. Achernar in the central Transantarctic Mountains offer at least ~500-400 ka and likely ~1 Ma of paleoglaciologic history for the edge of the EAIS plateau. Blue-ice moraines represent — for time periods in which they are preserved — relatively constant EAIS outlet glacier conditions and quasi-equilibrium forms. The observations support surface elevation changes associated with the Law Glacier of a minimum of ~50 m over at least the last two glacial cycles. A relatively stable central EAIS occurred during MIS 5, in terms of ice surface elevation, which left older MIS 6+ geomorphology and sediments intact. Our findings are consistent with those of other blue-ice studies around Antarctica (e.g., Fogwill et al., 2012). Disturbances to the Achernar blue-ice moraine did occur, but the magnitude of change was limited. The largest obvious disturbance was when the nearby Lewis Cliffs Ice Tongue was expanded, close to or prior to 500-400 ka. Gaps in the blue-ice moraine record may be more evident prior to the last two glacial cycles. A slight increase in ice thickness or ice input seems associated with the global LGM around ~20 ka and during the earliest Holocene, 9.2±0.5 ka. Sediments that recently reached the Law Glacier surface contain negligible inheritance in the context of the older moraine dating.

We ask the following questions specifically in terms of the Mt. Achernar record. However, the answers will provide a better context and understanding of blue-ice moraines as important paleoglaciologic archives around Antarctica. When did sediments start to accumulate at Mt. Achernar? What magnitude and rate of surface change disturbs moraine architecture, especially relative to subglacial flow and bedrock elevation? What caused the Lewis Cliffs Ice Tongue to expand and disturb the Law Glacier moraine sequence, and was it due to MIS 11 local climatic conditions? What caused debris to increase substantially below surfaces exposed >20 ka, and especially >50 ka, and are these particular times random? What determines the location of debris-loaded bands or planes? We infer ridge preservation and location of debris planes may be due to glacier surface history, how basal material is sub-glacially entrained, and thereafter how flow occurs relative to bedrock topography and structure. Another possibility is that englacial concentrations are dependent on where debris is derived, perhaps at specific places along the bed, with higher amounts associated with closer sources. Future modeling-based studies can also provide additional insights into blue-ice moraine processes.

Acknowledgements

This work was supported by National Science Foundation Antarctic grants PLR-1443433, PLR-1443213, ANT-0944578 and ANT-0944475. We thank the Polar Geospatial Center and UNAVCO (Marianne Okal, Annie Zaino, Joe Petit), the US Antarctic Program, Kenn Borek Air, Ltd., Michael Roberts and Peter Braddock and all other field team members from the

2010/11 and 2015/16 seasons. We also thank all personnel at the Center of Accelerator Mass Spectrometry (CAMS) at Lawrence Livermore National Laboratory and PRIME Lab for analyses. We thank Jean Hanley and Jeremy Frisch for laboratory assistance. As Reviewers, David Sugden and Peter Almond substantially improved the clarity and strength of the manuscript.

References

Akçar, N., Yeşilyurt, S., Hippe, K., Christl, M., Vockenhuber, C., Yavuz, V., Özsoy, B., 2020. Build-up and chronology of blue ice moraines in QueenMaud Land, Antarctica, Quaternary Science Advances, 2, 100012.

Ackert, R. P., 2000. Antarctic glacial chronology: new constraints from surface exposure dating, PhD thesis, Woods Hole Oceanographic Institution, Massachusetts Institute of Technology, pp. 213.

Ackert, R.P., Jr., Putnam, A.E., Mukhopadhyay, S., Pollard, D., DeConto, R.M., Kurz, M.D., Borns, H.W., Jr., 2013. Controls on interior West Antarctic Ice Sheet elevations: Inferences from geologic constraints and ice sheet modeling. Quaternary Science Reviews, 65, 26–38, doi:10.1016/j.quascirev.2012.12.017.

Bader, N.A., Licht, K.J., Kaplan, M.R., Kassab, C., Winckler, G., 2017. East Antarctic ice sheet stability recorded in a high-elevation ice-cored moraine. Quaternary Science Reviews, 159, 88-102.

Balco, G., Stone, J.O, Lifton, N.A., Dunai, T.J., 2008. A complete and easily accessible means of calculating surface exposure ages or erosion rates from ^{10}Be and ^{26}Al measurements. Quaternary Geochronology, 3, 174-195.

Balco, G., 2020. Noncosmogenic helium-3 in pyroxene and Antarctic exposure dating, https://cosmognosis.wordpress.com/2020/08/22/noncosmogenic-helium-3-in-pyroxene-and-antarctic-exposure-dating/.

Balter-Kennedy, A., Bromley, G., Balco, G., Thomas, H., Jackson, M. S., 2020. A 14.5-million-year record of East Antarctic Ice Sheet fluctuations from the central Transantarctic Mountains, constrained with cosmogenic ^{3}He, ^{10}Be, ^{21}Ne, and ^{26}Al.The Cryosphere, 14, 2647–2672, https://doi.org/10.5194/tc-14-2647-2020.

Bintanja, R., 1999. On the glaciological, meteorological and climatological significance of Antarctic blue ice area. Reviews of Geophysics, 37, 337–359.

Blackburn, T., Edwards, G., Tulaczyk, S., Scudder, M., Piccione, G., Hallet, B., McLean, N.M., Zachos, J., Cheney, B., Babbe, J., 2020. Ice retreat in Wilkes Basin of East Antarctica during a warm interglacial. Nature, 583, i.7817.

Borchers, B., Marrero, S., Balco, G., Caffee, M., Goehring, B., Lifton, N., Nishiizumi, K., Phillips, F., Schaefer, J., Stone, J., 2016. Geological calibration of spallation production rates in the CRONUS-Earth project. Quat. Geochronol. 31, 188–198.

Bromley, G.R.M., Hall, B.L., Stone, J.O., Conway, H., 2012. Late Pleistocene evolution of Scott Glacier, southern Transantarctic Mountains: implications for the Antarctic contribution to deglacial sea level. Quaternary Science Reviews, 50, 1-13.

Bromley, G.R.M., Winckler, G., Schaefer, J.M., Kaplan, M.R., 2014. Pyroxene separation by HF leaching and its impact on helium isotopes. Quaternary Geochronology, 23, 1-8.

Campbell, S., Balco, G., Todd, C., Conway, H., Huybers, K., Simmons, C., Vermeulen, M., 2013. Radar-detected englacial stratigraphy in the Pensacola Mountains, Antarctica: Implications for recent changes in ice flow and accumulation. Annals of Glaciology, 54, 91–100.

Cassidy, W., Harvey, R., Schutt, J., Disle, G., Yanai, K., 1992. The meteorite collection sites of Antarctica: Meteroritics, v. 27, p. 490–525, doi:10.1111/j.1945-5100.1992.tb01073.x.

Chinn, T.J., 1991. Polar glacier margin and debris features. Memorie della Societa Geologica Italiana, 46, 25–44.

Chinn, T.J., 1994. Glacier disequilibrium in the Convoy Range, Transantarctic Mountains, Antarctica. Institute of Geological & Nuclear Sciences Contribution, 217, 269–276.

Corti, G., Zeoli, A., Belmaggio, P., Folco, L., 2008. Physical modeling of the influence of bedrock topography and ablation on ice flow and meteorite concentration in Antarctica. Journal of Geophysical Research 113(F1), doi:10.1029/2006JF000708.

DeConto, R.M., Pollard, D., 2016. Contribution of Antarctica to past and future sea-level rise. Nature, 531, 591–597, doi:10.1038/nature17145.

Denton, G.H., Bockheim, J.G., Wilson, S.C., Leide, J.E., 1989. Late Quaternary ice surface fluctuations of Beardmore Glacier, Transantarctic Mountains. Quaternary Research 31, 183-209.

Denton, G.H., Anderson, R.F., Toggweiler, J.R., Edwards, R.L., Schaefer, J.M., Putnam, A.E., 2010. The last glacial termination. Science 328, 1652-1656.

Denton, G.H., Sugden, D.E., Marchant, D.R., Hall, B.L., Wilch, T.I., 1993. East Antarctic Ice Sheet sensitivity to Pliocene climatic change from a Dry Valleys perspective. Geografiska Annaler Series A, 75, 155-204.

Denton, G.H., Putnam, A.E., Russell, J.L., Barrell, D.J.A., Schaefer, J.M., Kaplan, M.R., Strand, P.D., 2021. The Zealandia Switch: Ice age climate shifts viewed from Southern Hemisphere moraines. Quaternary Science Reviews. 257, 106771.

Doughty, A.M., Kaplan, M.R., Peltier, C., Barker, S., 2021. A global maximum in glacier extent during MIS 4. Quaternary Science Reviews, 261, 106948.

Eaves, S.R., Winckler, G., Schaefer, J.M., Vandergoes, M.J., Alloway, B.V., Mackintosh, A.N., Townsend, D.B., Ryan, M.T., Li, X., 2015. A test of the cosmogenic 3He production rate in the south-west Pacific (39°S). Journal of Quaternary Science, 30, 79-87.

Eaves, S.R., Mackintosh, A.N., Winckler, G., Schaefer, J.M., Alloway, B.V., Townsend, D.B., 2016. A Cosmogenic ^{3}He chronology of late Quaternary glacier fluctuations in North Island, New Zealand (39°S). Quaternary Science Reviews, 132, 40-56.

Faure, G., Mensing, T.M., Johnson, K.S., 1992. Composition of rock clasts in the Mt. Achernar moraine and the Lewis Cliff ice tongue. Antarctic Journal, U. S. 11-12.

Fogwill, C.J., Hein, A.S., Bentley, M.J., Sugden, D.E., 2012. Do blue-ice moraines in the Heritage Range show the West Antarctic ice sheet survived the last interglacial? Palaeogeography, Palaeoclimatology, Palaeoecology, 335–336, 61–70.

Golledge, N.R. and 12 others, 2013. Glaciology and geological signature of the Last Glacial Maximum Antarctic ice sheet. Quaternary Science Reviews, 78, 225–247.

Graly, J.A., Licht, K.J., Drushel, G.K., Kaplan, M.R., 2018a. Polar desert chronologies through quantitative measurements of salt accumulation. Geology, 46, 351-354.

Graly, J.A., Licht, K.J., Kassab, C.M., Bird, B.W. Kaplan, M.R., 2018b. Warm-based basal sediment entrainment and far-field Pleistocene origin evidenced in central Transantarctic blue ice through stable isotopes and internal structures. Journal of Glaciology 64, 185-196.

Graly, J.A., Licht, K.J., Bader, N.A. Bish, D.L., 2020. Chemical weathering signatures from Mt. Achernar Moraine, Central Transantarctic Mountains I: Subglacial sediments compared to underlying rock. Geochimica et Cosmochimica Acta, 283, 149-166.

Hagen, E.H., 1995. A geochemical and petrological investigation of meteorite ablation products in till and ice of Antarctica [Ph.D. Thesis]: Columbus, The Ohio State University, 525 p.

Hall, B.L., Denton, G.H., Stone, J.O., Conway, H., 2013. History of the Grounded Ice Sheet in the Ross Sea Sector of Antarctica during the Last Glacial Maximum and the Last Termination. 381, Geological Society, London, pp. 167-181. Special Publication.

Hein, A., et al., 2016. Evidence for the stability of the West Antarctic Ice Sheet divide for 1.4 million years, Nature Communications, 7, 10325–10332, doi:10.1038/ncomms10325.

Higgins, J.A., Kurbatov, A.V., Spaulding, N.E., Brook, E., Introne, D.S., Chimiak, L.M., Yan, Y., Mayewski, P.A., Bender, M.L., 2015. Atmospheric composition 1 million years ago from blue ice in the Allan Hills, Antarctica, Proceedings of the National Academy of Sciences, 112 6887-6891.

Howat, I. M., Porter, C., Smith, B. E., Noh, M.-J., Morin, P., 2019. The Reference Elevation Model of Antarctica, The Cryosphere, 13, 665-674, https://doi.org/10.5194/tc-13-665-2019.

Joy, K., Fink, D., Storey, B., Atkins, C., 2014. A 2 million year glacial chronology of the Hatherton Glacier, Antarctica and implications for the size of the East Antarctic Ice Sheet at the Last Glacial Maximum. Quaternary Science Reviews, 83, 46–57.

Kaplan, M.R., Strelin, J.A., Schaefer, J.M., Denton, G.H., Finkel, R.C., Schwartz, R., Putnam, A.E., Vandergoes, M.J., Goehring, B.M., Travis, S.G., 2011. In-situ cosmogenic ^{10}Be production rate at Lago Argentino, Patagonia: Implications for late-glacial climate chronology. Earth and Planetary Science Letters, 309, 21–32.

Kaplan, M.R., Licht, K.J., Winckler, G., Schaefer, J.M., Bader, N., Mathieson, C., Roberts, M., Kassab, C.M., Schwartz, R., Graly, J.A., 2017. Mid-Late Pleistocene stability of the central East Antarctic Ice Sheet at the head of Law Glacier. Geology, 45, 963-966.

Kassab, C.M., Licht, K.J., Petersson, R., Lindbäck, K., Graly, J.A., Kaplan, M.R., 2020. Formation and evolution of an extensive blue ice moraine in central Transantarctic Mountains, Antarctica. Journal of Glaciology 66, 49-60.

Lal, D., 1991. Cosmic-ray labeling of erosion surfaces in-situ nuclide production rates and erosion models. Earth and Planetary Science Letters, 104, 424-439.

Lamp, J.L, Marchant, D.R., 2017. Vapor transport and sublimation on Mullins Glacier, Antarctica. Earth and Planetary Science Letters 465, 82-91.

Lisiecki, L.E., Raymo, M.E., 2005. A Pliocene-Pleistocene stack of 57 globally distributed benthic delta O-18 records. Paleoceanography 20.

Lifton, N., Sato, T., Dunai, T., 2014. Scaling in situ cosmogenic nuclide production rates using analytical approximations to atmospheric cosmic-ray fluxes. Earth and Planetary Science Letters 386 149-160.

Mercer, J.H., 1968. Glacial geology of the Reedy glacier area, Antarctica. Geological Society of America Bulletin, 79, 471-486.

Palmer, E.F., Licht, K.J., Swope, R.J., Hemming, S.R., 2012. Nunatak moraines as a repository of what lies beneath the East Antarctic ice sheet. In: Rasbury, E.T., Hemming, S.R., Riggs, N.R. (Eds.), Mineralogical and Geochemical Approaches to Provenance, 487. Geological Society of America Special Paper, pp. 97-104.

Pattyn, R. 2010. Antarctic subglacial conditions inferred from a hybrid ice sheet/ice stream model. Earth and Planetary Science Letters 295, 451–461.

Putnam, A., Schaefer, J., Barrell, D.J.A., Vandergoes, M., Denton, G.H., Kaplan, M., Finkel, R.C., Schwartz, R., Goehring, B.M., Kelley, S., 2010. In situ cosmogenic ^{10}Be production-rate calibration from the Southern Alps, New Zealand. Journal of Quaternary Geochronology, 5, 392–409.

Scarrow, J.W., Balks, M.R., Almond, P.C., 2014. Three soil chronosequences in recessional glacial deposits near the polar plateau, in the Central Transantarctic Mountains, Antarctica. Antarctic Science 26, 573-583.

Schäfer, J. M., S. Ivy-Ochs, R. Wieler, I. Leya, H. Baur, G. H. Denton, C. Schlüchter, 1999. Cosmogenic noble gas studies in the oldest landscape on earth: surface exposure ages of the Dry Valleys, Antarctica. Earth and Planetary Science Letters, 167, 215-226.

Schaefer, J.M., Denton, G.D., Kaplan, M.R., Putnam, A., Finkel, R.C., Barrell, D.J.A., Andersen, B.G., Schwartz, R., Mackintosh, A., Chinn, T., Schlüchter, C., 2009. High frequency Holocene glacier fluctuations in New Zealand differ from the northern signature. Science 324, 622–625.

Sinisalo, A., Moore, J.C., 2010. Antarctic blue ice areas – towards extracting paleoclimate information. Antarctic Science, 22, 99–115.

Stone, J.O., 2000. Air pressure and cosmogenic isotope production. Journal Geophysical Research, 105, 23753-23759.

Sun, T., Socki, R.A., Bish, D.L., Harvey, R.P., Bao, H., Niles, P.B., Cavicchioli, R., and Tonui, E., 2015. Lost cold Antarctic deserts inferred from unusual sulfate formation and isotope signatures. Nature Communications, 6, 7579, doi:10.1038/ncomms8579.

Todd, C., Stone, J. O. H., Conway, H., Hall, B., Bromley, G., 2010. Late Quaternary evolution of Reedy Glacier, Antarctica. Quaternary Science Reviews, 29, 1328–1341.

Westoby, M.J., Dunning, S.A., Woodward, J., Hein, A.S., Marrero, S.M., Winter, K., Sugden, D.E., 2016. Interannual surface evolution of an Antarctic blue-ice moraine using multi-temporal DEMs. Earth Surface Dynamics, 4, 515-529.

Whillans, I.M., Cassidy, W.A., 1983. Catch a falling star: Meteorites and old ice. Science, 222, 55–57, doi:10.1126/science.222.4619.55.

Whitehouse, P.L., Bentley, M.J., Le Brocq, A.M. 2012. A deglacial model for Antarctica: geological constraints and glaciological modelling as a basis for a new model of Antarctic glacial isostatic adjustment. Quaternary Science Reviews 32, 1–24.

Woodward, J., Hein, A., Winter, K., Westoby, M., Marrero, S., Dunning, S., Lim, M., Rivera, A. Sugden, D., 2022. Blue-ice moraines formation in the Heritage Range, West Antarctica:

Implications for ice sheet history and climate reconstruction., Quaternary Science Advances, 6, 100051.

Figure Captions.

Figure 1. Setting of the Mt. Achernar area. A) Mt. Achernar moraine sits at the head of Law Glacier (within red box) where unconstrained flow off of the East Antarctic plateau becomes constrained through Transantarctic Mountains. B) Ice surface velocities and sediment catchment area for the Mt. Achernar area (Bader et al. 2017; Graly et al., 2018b). C) The entire moraine complex along with locations of sediment (till) samples for study of provenance changes (Bader et al., 2017) and soil geochemistry (Graly et al., 2017). Also shown are zones (in white) defined in Bader et al. (2017), the general area of study by Scarrow et al. (2014), and ice flow directions with arrows. Note the ice flow is steered away from the main trunk glacier, where it is then trapped in the embayment (Kassab et al. 2020). D) Image of the Achernar moraine and surrounding area, from Antarctic REMA (Reference Elevation Model of Antarctica) Explorer (Howat et al., 2019).

Figure 2. All ^{10}Be-^{26}Al-^{3}He ages obtained in the Mt. Achernar area. A) The study area including the tail area (NW sector), which is shown in more detail in Figure 5. The yellow-dashed line outlines moraine associated with the Lewis Cliffs Ice Tongue, which impinged on and disturbed the Mt. Achernar blue-ice moraine. We show the two oldest boron-exposure ages (Graly et al., 2018a) (Fig. 1C), in the southwestern sector, to the right of Lewis Cliffs Ice Tongue. B) A focus on the main and lateral moraine areas, which are shown in more detail in Figures 3 and 4. Italicized ages are discussed as outliers. All exposure ages are on boulders except those labelled 'c' (cobble-size). All ages in ka, except for three 10Be ages in pink (years), which are on samples from the

Law Glacier margin (see next, Figure 3 for more detail). Yellow-dashed lines with associated ages mark approximate age boundaries.

Figure 3. Focus on the best-dated Zones 1 and 2, looking west with the Law Glacier on the right. Headwall of Mt. Achernar shown in background. Four ^{10}Be ages on samples along the lateral moraine, date to 9.2 ± 0.5 ka and record a high surface for ice flowing off the plateau, which is seen in the upper right. GPR radargram profile below the photo is from Kassab et al. (2020), and more or less follows the yellow-dashed line. Dipping stacked and scatterred hyperbolas are inferred to represent planes of debris and cobbles/boulders causing point reflectors, respectively. Figure 6 provides additional photos of the lateral moraine with samples.

Figure 4. Similar to Figure 3, with photos focusing on Zones 2 to 4 and cosmogenic exposure ages. Top panel focuses on Zone 2, with the Law Glacier (Fig. 3) on right side. Middle panel focuses on Zones 2 and 3 including moraines dated to MIS 2 time; the average and standard deviation are 19.3±0.8 ka excluding the one outlier of 5.9±0.1. Bottom panel focuses on inner Zone 4 and samples dating to <100 ka. Mt Achernar headwall is in the background. In each subsequent panel, some overlap in exposure ages is shown on right side.

Figure 5. A focus on the tail area, with view looking southwest, towards Mt. Achernar. Law Glacier is on the right. Note relatively oxidized sediments on the left side of the photo, which date to MIS 6 and 5 except for 1 outlier of ~18.6 ka. Also shown are MIS 5 ages (~135.2 to ~86.1 ka) from the main area of focus (Fig. 2B), which is in the background. All are boulder ages except if labelled "c" (cobble size). Two outliers are italicized. See Figure 6 for photos that focus on the right side

of image; both the ~0.3 and ~0.9 ka ages are slightly closer to the present margin, compared with the ~1.1 and ~2.7 ka ages.

Figure 6. Photos that provide context of geomorphology and age data. A) Three 10Be ages near the moraine/ Law Glacier boundary. Person for scale. In this panel the three ages are in years, in all other panels they are in ka. B) and C) A focus on the tail area and samples MAR-15-87 (ice margin) and -88 (+4 m). D) The lateral moraine, with two apparent ridges. E) The lateral moraine and trimline, close to (NW of) sample MAR-15-92c (panel G). The tallest boulders are ~1 m in height and we estimate the trimline is about 15-20 m higher. F) The lateral moraine and trimline, by MAR-15-98c (panel G). We estimate the trimline is <10 m higher. G) The area near the lateral moraine with ^{10}Be ages (all cobbles). We also show the elevation difference between the Law Glacier (1858 m), lateral moraine (~1905 m), and towards the south (1868 m). Note the area next to the lateral moraine is smoother without distinct ridges, as exists to the left (east) closer to the area of the main transect (white-dashed line, Fig. 2). We infer disturbances within ~500 m of the lateral moraine due to the rise in surface by ~10-9 ka and when the trimline formed.

Figure 7. ^{10}Be-^{3}He-Boron exposure ages with distance from the Law Glacier along the main transect (white-dashed line, Fig. 2). **Panels A, B**) Left side is plotted as log-log plot. Three respective exponential relations demonstrate there is a steady increase in age from the active margin. Within ~2200 m (~50 ka) from the Law Glacier, if the relation is represented by a linear line, the r^2 is ~0.8 (^{10}Be) or ~0.6 (^{3}He). Boron ages are from Graly et al. (2018a). Circle marks younger sediment dated, where ^{10}Be-^{26}Al-Boron exposure ages all indicate exposure for less time.

In panel B, approximate average accretion rate based on ^{10}Be and the two oldest Boron ages at ~5600-6100 m. **Panels C, D)** Topographic profiles from Bader et al. (2017) and Kaplan et al. (2017). In panel C, the ages from Hagen (1995) are at the bottom because it is not clear how they align with the main transect. MIS labels are approximately located with distance. For simplicity, ^{26}Al ages are not shown. In Panel D, Zones 1 to 3 (Z1-Z3) are shown along bottom.

Figure 8. Plot of ^{26}Al/^{10}Be ratios versus ^{10}Be concentrations, with data colored in blue and red from Hagen (1995) and Kaplan et al. (2017), respectively, recalculated with updated systematics. MAR-11-22 is not shown on the plot due to its high ^{26}Al/^{10}Be value (Table 1). The first and last parts of each sample name are shown next to analyses. The ratios are standardized (*) to 6.75, the Be-10 concentrations are relative to 07KNSTD and sea level high latitude (Balco et al., 2008). Error bars are 1σ analytical uncertainty.

Figure 9. Ground Penetrating radar (GPR, 25MHz) with approximate locations of ^{10}Be-^{3}He above the topographically corrected surface. Ages are shifted slightly so as to be at their approximate location along GPR transect. The upper panel is the processed radargram and the lower panel has interpretations including red-dashed lines as debris planes. Kassab et al. (2020) interpreted the blue-dashed line, which represents a continuous subhorizontal reflector, to be the bedrock surface at ~140 m to >220 m below. Above the GPR data, we show both maximum sediment entrainment age (Graly et al., 2020, Kassab et al. 2020) and surface exposure ages. Boundaries between MIS are fuzzy given ranges of ages. Kassab et al. (2020) also presented GPR analyses for inner Zone 4, with exposure ages ≥100ka, but they found a lack of consistent GPR reflections. For simplicity, ^{26}Al ages are not shown.

Figure 10. ^{10}Be-^{26}Al-^{3}He ages compared with benthic δ^{18}O stack (Lisiecki and Raymo, 2004). Top panels include ages with St/Lm scaling (difference not discernable at the scale shown). During MIS 5, a concentration of ages occurs at 120-100 ka excluding "outlier' ages <90 ka from the same sites (Fig. 5). Taken at face value these ages overlap with MIS5c or 5c-d. Bottom panels include exposure ages calculated with the LSDn scaling (Table 1,3) method, which are ~10-12% lower than those calculated using St/Lm.

Table 1. Geographical and Analytical details for ^{10}Be and ^{26}Al samples

Sample ID	Latitude (DD)	Longitude (DD)	Elevation (masl)[a]	Sample Thickness (cm)	Shielding correction	Quartz weight (g)	Carrier (Be) Added (g)	$^{10}Be/^{9}Be \pm 1\sigma^{b}$	$[^{10}Be] \pm 1\sigma$ (atoms x g^{-1})	$^{26}Al/^{27}Al \pm 1\sigma^{b}$	Total Al	$[^{26}Al] \pm 1\sigma$ (atoms x g^{-1})	$^{26}Al/^{10}Be \pm 1\sigma$
MAR-11-22	-84.1886	161.2649	1823.14	0.61	0.999	3.0517	0.1868	8.2943E-14 ± 1.8425E-15	338030 ± 7523	2.2501E-13 ± 1.7538E-14	1.9849	3.2401E+06 ± 2.5254E+05	9.6
MAR-11-10	-84.2216	161.3567	1847.24	1.07	1.000	10.5039	0.1870	3.6375E-12 ± 5.2707E-14	4505087 ± 65279	1.3026E-11 ± 2.3824E-13	1.0860	3.1280E+07 ± 5.7209E+05	6.9
MAR-11-18	-84.1906	161.2829	1825.41	1.05	0.999	16.8605	0.1874	1.4726E-13 ± 2.7890E-15	121259 ± 2298	3.1385E-13 ± 2.3831E-14	1.9681	9.0289E+05 ± 6.8557E+04	7.4
MAR-11-26	-84.2086	161.3498	1837.80	1.67	1.000	6.8121	0.1873	3.4409E-12 ± 4.8423E-14	4291924 ± 60401	7.9704E-12 ± 2.0844E-13	1.7343	3.0733E+07 ± 8.0373E+05	7.2
MAR-11-30	-84.198	161.2619	1836.72	1.07	0.997	7.1486	0.1881	8.5767E-13 ± 2.0059E-14	1258430 ± 29433	2.2938E-12 ± 5.3104E-14	1.4846	8.8623E+06 ± 2.0517E+05	7.0
MAR-11-37	-84.2008	161.3199	1832.74	1.36	0.999	10.0921	0.1848	2.0383E-12 ± 2.5791E-14	2485394 ± 31448	4.2631E-12 ± 8.2534E-14	1.8284	1.7165E+07 ± 3.3232E+05	6.9
BLANK_1_2012May01							0.1871	3.4685E-16 ± 1.1828E-16		3.6006E-15 3.6006E-15	1.0131		
BLANK_2_2012May01							0.1846	3.1379E-16 ± 1.0460E-16			1.6752		
					average=		0.1859	3.3032E-16 ± 1.1144E-16					
MAR-11-14a	-84.2194	161.3374	1845.51	2.02	1.000	4.0553	0.1838	3.9103E-12 ± 4.2992E-14	11841897 ± 130214	7.2650E-12 ± 1.3529E-13	1.6752	6.6932E+07 ± 1.2464E+06	5.7
MAR-11-14b	-84.2194	161.3374	1845.51	3.02	1.000	4.0632	0.1852	3.8754E-12 ± 4.2663E-14	11798825 ± 129907	7.3518E-12 ± 1.3708E-13	1.6917	6.8267E+07 ± 1.2729E+06	5.8
MAR-11-17	-84.1907	161.282	1825.76	1.10	0.999	5.0766	0.1875	6.4713E-14 ± 1.7348E-15	154713 ± 4481	1.8906E-13 ± 1.9192E-14	1.2010	9.5426E+05 ± 9.6869E+04	6.2
MAR-11-33	-84.197	161.2506	1836.37	1.87	0.999	8.0920	0.1868	5.9276E-13 ± 7.6799E-15	911557 ± 11861	1.3267E-12 ± 4.4710E-14	1.5731	5.7292E+06 ± 1.9308E+05	6.3
Blank_2_2013Jan24							0.1833	2.1064E-15 ± 7.0965E-16		6.9381E-15 ± 4.9072E-15	1.4472		
MAR-15-63	-84.1815	161.2797	1805.76	2.02	0.99	71.3604	0.1881	1.2475E-14 ± 6.0648E-16	1945 ± 116	1.8808E-01 ± 1.2572E+19			
MAR-15-89	-84.1011	162.13	1726.54	2.90	0.99	68.2679	0.1894	1.8575E-12 ± 2.2055E-14	344253 ± 4088	1.8942E-01 ± 1.2662E+19			
BLK1-2017Jan20							0.1901	7.4243E-16 ± 2.6619E-16		1.9015E-01 ± 1.2710E+19			
BLK2-2017Jan20							0.1894	2.1044E-15 ± 6.0420E-16		1.8942E-01 ± 1.2662E+19			
					average=		0.1898	1.4234E-15 ± 4.3520E-16		1.8979E-01 ± 1.2686E+19			
MAR-15-57	-84.1869	161.2382	1825.56	1.30	0.99	5.0465	0.2094	1.0989E-13 ± 2.1170E-15	302471 ± 5855	2.0939E-01 ± 1.3996E+19			
MAR-15-58	-84.1869	161.2344	1822.93	1.15	0.99	5.1301	0.2102	9.8471E-14 ± 1.8819E-15	267457 ± 5142	2.1022E-01 ± 1.4052E+19			
MAR-15-59	-84.1851	161.2603	1821.98	4.25	0.99	9.1888	0.2108	9.5336E-14 ± 1.7955E-15	144958 ± 2748	2.1084E-01 ± 1.4093E+19			
Blk1-2017Mar31							0.2108	8.5073E-16 ± 2.2658E-16		2.1084E-01 ± 1.4093E+19			
Blk2-2017Mar31							0.2111	1.0428E-15 ± 2.4995E-16		2.1105E-01 ± 1.4107E+19			
MAR-15-62	-84.183	161.2835	1811.08	1.16	0.99	11.8519	0.2112	8.6337E-14 ± 2.4524E-15	101838 ± 2903	2.1116E-01 ± 1.4114E+19			
MAR-15-107	-84.1828	161.2698	1823.27	1.79	0.99	10.0178	0.2111	5.8470E-14 ± 1.5704E-15	81180 ± 2199	2.1105E-01 ± 1.4107E+19			
MAR-15-108	-84.1826	161.2707	1823.27	1.48	0.99	10.0021	0.2107	5.3998E-14 ± 1.5487E-15	74888 ± 2167	2.1074E-01 ± 1.4086E+19			
Blk3-2017Mar31							*0.2109*	*6.5596E-15 ± 5.1785E-16*		*2.1095E-01 ± 1.4100E+19*			
Blk4-2017Mar31							0.2109	5.7627E-16 ± 1.4250E-16		2.1095E-01 ± 1.4100E+19			
					average=		0.2109	8.2327E-16 ± 2.0634E-16		2.1095E-01 ± 1.4100E+19			
MAR-15-101	-84.187	161.2673	1819.72	0.88	0.99	5.0128	0.2112	8.1879E-14 ± 1.8060E-15	229013 ± 5068	2.1119E-01 ± 1.4116E+19			
MAR-15-102	-84.1887	161.2869	1824.17	1.45	0.99	5.0146	0.2106	1.2888E-13 ± 2.4900E-15	360163 ± 6971	2.1057E-01 ± 1.4075E+19			
MAR-15-105	-84.1872	161.2756	1819.72	1.14	0.99	5.0264	0.2116	1.0568E-13 ± 2.4496E-15	295833 ± 6869	2.1161E-01 ± 1.4144E+19			
MAR-15-110	-84.1823	161.2723	1823.27	1.56	0.99	10.264	0.2117	1.1291E-14 ± 5.7741E-16	14802 ± 781	2.1171E-01 ± 1.4151E+19			
Blk-2017Apr24							0.2115	5.5490E-16 ± 1.4507E-16		2.1150E-01 ± 1.4137E+19			
MAR-15-123	-84.2057	161.3475	1843	1.93	0.99	5.0634	0.2110	7.6295E-13 ± 1.1594E-14	2123403 ± 32269	2.1098E-01 ± 1.4103E+19			
MAR-15-124	-84.2056	161.3488	1848	0.99	0.99	5.0628	0.2113	1.0646E-12 ± 2.1445E-14	2968196 ± 59794	2.1129E-01 ± 1.4123E+19			
MAR-15-127	-84.193	161.285	1826.45	0.82	0.99	5.0203	0.2118	1.6935E-13 ± 3.2120E-15	476029 ± 9038	2.1181E-01 ± 1.4158E+19			
MAR-15-129	-84.1928	161.2845	1826.45	0.51	0.99	5.1102	0.2116	5.4337E-14 ± 1.2848E-15	148861 ± 3542	2.1161E-01 ± 1.4144E+19			
MAR-15-130	-84.193	161.2735	1831.73	0.97	0.99	5.2448	0.2115	1.7745E-13 ± 3.2912E-15	476819 ± 8852	2.1150E-01 ± 1.4137E+19			
MAR-15-61*	-84.1852	161.2618	1821.98	3.55	0.99	2.2905	0.2108	1.1178E-14 ± 2.6466E-15	67678 ± 16096	2.1075E-01 ± 1.4087E+19			
MAR-15-92*	-84.1783	160.988	1904.60	4.00	0.96	2.6515	0.2113	4.0871E-14 ± 2.2903E-15	216753 ± 12219	2.1127E-01 ± 1.4122E+19			
MAR-15-96*	-84.193	161.0739	1867.90	3.58	0.97	3.8038	0.2109	6.5878E-14 ± 4.0279E-15	243455 ± 14914	2.1086E-01 ± 1.4094E+19			
MAR-15-113*	-84.2194	161.3371	1845.51	2.03	0.99	2.4022	0.2110	1.4587E-12 ± 2.4562E-14	8561925 ± 144173	2.1096E-01 ± 1.4101E+19			
MAR-15-115*	-84.1185	161.905	1744.06	1.38	0.99	5.1354	0.2109	8.9057E-13 ± 1.8826E-14	2443724 ± 51663	2.1086E-01 ± 1.4094E+19			
MAR-15-116*	-84.1185	161.9035	1744.06	0.97	0.99	5.1346	0.2108	8.8475E-13 ± 2.5301E-14	2426941 ± 69401	2.1075E-01 ± 1.4087E+19			
MAR-15-117*	-84.12	161.8898	1740.26	1.37	0.99	5.0444	0.2101	8.4521E-13 ± 1.9706E-14	2352964 ± 54862	2.1013E-01 ± 1.4046E+19			
MAR-15-118*	-84.1201	161.8926	1740.26	2.2	0.99	5.5238	0.2104	1.6919E-13 ± 5.6893E-15	430398 ± 14487	2.1044E-01 ± 1.4067E+19			
BLK-2017May10							0.2111	1.7418E-16 ± 2.5100E-16		2.1107E-01 ± 1.4108E+19			
MAR-15-121*	-84.1185	161.9035	1744.06	4.58	0.99	5.0141	0.2105	6.8561E-13 ± 1.2952E-14	1923867 ± 36351	2.1055E-01 ± 1.4074E+19			

MAR-15-64	-84.1814	161.2815	1807.76	5.17	1.00	60.2190	0.1881	6.6579E-15 ± 4.5087E-16	1244 ± 85	1.8806E-01 ± 1.2570E+19
MAR-15-65	-84.145	161.6559	1807.76	5.03	1.00	60.3486	0.1889	9.5706E-15 ± 1.0482E-15	1857 ± 204	1.8889E-01 ± 1.2626E+19
MAR-15-111	-84.1818	161.2609	1822	5.42	1.00	59.0633	0.1894	1.1843E-13 ± 2.7978E-15	25238 ± 596	1.8941E-01 ± 1.2660E+19
Blk1-2018Apr12							0.1882	6.9705E-16 ± 4.8794E-17		1.8816E-01 ± 1.2577E+19
MAR-15-142-T	-84.108	162.0283	1735.46	1.2	1.00	25.1410	0.1884	1.2708E-13 ± 2.9053E-15	63450 ± 1452	1.8840E-01 ± 1.2593E+19
MAR-15-143	-84.1079	162.0362	1735.53	2.17	1.00	25.0331	0.1888	4.0044E-14 ± 9.7898E-16	19986 ± 493	1.8881E-01 ± 1.2621E+19
MAR-15-139	-84.1784	161.546	1765.28	2.23	1.00	15.0371	0.1886	2.2616E-14 ± 7.7663E-16	18623 ± 649	1.8861E-01 ± 1.2607E+19
MAR-15-142-H	-84.1793	161.5309	1762.27	1.47	1.00	15.0697	0.1888	2.0394E-14 ± 8.0085E-16	16743 ± 666	1.8881E-01 ± 1.2621E+19
MAR-15-145	-84.1711	161.6566	1753.73	1.11	1.00	15.3124	0.1886	1.8045E-13 ± 3.3488E-15	148239 ± 2753	1.8861E-01 ± 1.2607E+19
Blk1-2018May02							0.1886	4.5315E-16 ± 1.4450E-16		1.8861E-01 ± 1.2607E+19
MAR-15-132	-84.1016	162.1294	1734.24	1.91	1.00	15.6711	0.1886	2.1908E-14 ± 9.8354E-16	17301 ± 784	1.8861E-01 ± 1.2607E+19
MAR-15-133	-84.1016	162.1297	1733.24	2.39	1.00	4.0390	0.1886	1.2773E-14 ± 5.6459E-16	38610 ± 1752	1.8861E-01 ± 1.2607E+19
MAR-15-137	-84.0944	162.2205	1736	2.41	1.00	25.0135	0.1876	8.2752E-13 ± 1.3800E-14	414581 ± 6914	1.8757E-01 ± 1.2538E+19
MAR-15-94	-84.1826	161.0115	1894.53	4.22	0.96	25.2107	0.1889	4.7329E-13 ± 5.9397E-15	236863 ± 2973	1.8892E-01 ± 1.2628E+19
MAR-15-97	-84.1928	161.0732	1867.90	3.45	0.97	19.7066	0.1887	3.4883E-13 ± 5.9739E-15	223022 ± 3820	1.8871E-01 ± 1.2614E+19
Blk2-2018May02							0.1879	3.5369E-16 ± 1.1799E-16		1.8788E-01 ± 1.2558E+19
					average=			1.3124E-16		
MAR-15-76	-84.1401	161.6932	1743.05	5.13	1.00	68.8982	0.1858	7.0104E-15 ± 3.9843E-16	1094 ± 71	1.8582E-01 ± 1.2420E+19
MAR-15-87	-84.1068	162.0493	1731.42	5.00	1.00	71.2908	0.1858	4.2733E-14 ± 1.3147E-15	7280 ± 227	1.8582E-01 ± 1.2420E+19
MAR-15-88	-84.1414	161.6911	1760	4.29	1.00	70.6214	0.1858	1.4030E-13 ± 2.5992E-15	24507 ± 456	1.8582E-01 ± 1.2420E+19
BLK1-2019Jan31							0.1856	1.1055E-15 ± 2.1689E-16		1.8562E-01 ± 1.2406E+19
BLK2-2019Jan31							0.1853	7.8632E-16 ± 1.7585E-16		1.8531E-01 ± 1.2385E+19
					average=			1.9637E-16		

Notes: The first two sets of samples (n=10) above the horizontal black line are from Kaplan et al. (2017). Samples with asterisk – associated with blank BLK2017May10 – were analyzed at PRIME Lab, all others were analyzed at CAMS-LLNL. Given large uncertainty for MAR-15-61 (>20%), it is not used. Sample elevations to a whole number were measured with a handheld GPS, otherwise by differential GPS (Trimble). AMS standard used for normalization is $2.85x10^{-12}$=07KNSTD3110. Shown are 1σ analytical AMS uncertainties. Column of ^{9}Be added is adjusted for carrier (Be) concentration. Tables also are provided as Supplementary Material.

Table 2. Surface-exposure sample details and ^{3}He data.

Sample ID	Latitude (DD)	Longitude (DD)	Elevation (masl)[a]	Sample Thickness (cm)	Shielding correction	Pyroxene Mass (g)	$He^3/He^4 \pm 1\sigma$	$[^3He] \pm 1\sigma$ (atoms/g)	standard
MAR-11-08	-84.1910	161.2749	1829.79	1.07	0.999	0.0719	7.4858E+05 ± 8.690E-08	9.215E+06 ± 7.486E+05	MM
MAR-11-08						0.0312	8.7819E+05 ± 1.136E-07	1.073E+07 ± 8.782E+05	MM
MAR-11-08 avg								9.973E+06 ± 8.160E+05	
MAR-11-23	-84.1870	161.2414	1825.85	1.35	0.999	0.0460	1.0899E-07 ± 8.539E-09	8.317E+06 ± 5.385E+05	MM
MAR-11-23						0.0371	1.3302E-07 ± 9.684E-09	9.397E+06 ± 6.839E+05	MM
MAR-11-23 avg								8.857E+06 ± 6.155E+05	
MAR-11-52	-84.2286	161.2652	1830.53	1.09	0.999	0.0516	5.5264E+06 ± 9.438E-06	2.380E+08 ± 5.526E+06	MM
MAR-11-48Green	-84.2268	161.2755	1840.52	1.13	0.999	0.0254	2.2413E+06 ± 2.363E-06	8.237E+07 ± 2.241E+06	MM
MAR-11-48Red	-84.2268	161.2755	1840.52	1.13	0.999	0.0263	2.2742E+06 ± 3.169E-07	8.281E+07 ± 2.274E+06	MM
MAR-11-21AL	-84.1887	161.2672	1823.14	1.09	0.999	0.0285	9.4099E+05 ± 3.169E-07	1.769E+07 ± 9.410E+05	MM
MAR-11-21CM	-84.1887	161.2672	1823.14	1.09	0.999	0.0333	8.1605E+05 ± 2.744E-07	1.557E+07 ± 8.161E+05	MM
MAR-11-35	-84.2011	161.3220	1827.24	1.31	0.999	0.0315	1.9503E+06 ± 1.271E-06	7.354E+07 ± 1.950E+06	MM
MAR-11-01	-84.1790	161.5365	1765.28	1.29	0.999	0.0290	4.4749E+05 ± 6.990E-08	5.029E+06 ± 4.475E+05	MM
MAR-11-02	-84.1791	161.5366	1765.28	0.57	0.999	0.0227	5.5215E+05 ± 1.040E-07	5.076E+06 ± 5.522E+05	MM
MAR-11-09	-84.1911	161.2725	1829.28	1.00	0.999	0.0262	5.9883E+05 ± 1.093E-07	8.530E+06 ± 5.988E+05	MM
MAR-15-112	-84.1414	161.6911	1822	3.87	0.998	0.1250	4.1334E-08 ± 1.328E-09	1.296E+07 ± 4.063E+05	Air
MAR-15-112						0.1226	4.2506E-08 ± 1.125E-09	1.333E+07 ± 3.457E+05	Air
MAR-15-112_avg								1.315E+07 ± 3.772E+05	
MAR_15_120	-84.1190	161.8995	1744.06	1.68	0.990	0.2001	4.6848E-06 ± 7.864E-08	7.219E+07 ± 1.187E+06	MM
MAR_11_41	-84.1087	162.0593	1737.80	0.94	0.990	0.2002	6.0928E-07 ± 9.308E-09	1.096E+08 ± 1.444E+06	Air
MAR_11_42	-84.1087	162.0578	1737.80	1.10	0.990	0.2002	2.1186E-07 ± 3.354E-09	7.842E+07 ± 1.081E+06	Air
MAR_15_126	-84.2060	161.3452	1847	1.00	0.990	0.1993	9.8634E-07 ± 1.485E-08	1.360E+08 ± 1.761E+06	Air
MAR_15_119	-84.1198	161.8960	1740.26	1.06	0.990	0.5028	1.1002E-06 ± 1.638E-08	7.050E+07 ± 9.003E+05	Air
MAR_15_125_2	-84.2056	161.3483	1860	2.30	0.990	0.5008	3.1158E-06 ± 4.583E-08	1.021E+08 ± 1.281E+06	Air
MAR_15_128_2	-84.1930	161.2859	1826.45	2.16	0.990	0.5033	2.9126E-07 ± 4.954E-09	1.374E+07 ± 2.090E+05	Air
MAR_15_131_2	-84.1930	161.2720	1831.73	0.99	0.990	0.4975	3.4440E-07 ± 5.719E-09	1.533E+07 ± 2.264E+05	Air
MAR_11_13	-84.2209	161.3382	1847.94	1.09	0.990	0.2018	1.0618E-06 ± 1.556E-08	2.889E+08 ± 3.610E+06	Air
MAR_11_15	-84.2190	161.3443	1846.23	2.15	0.990	0.2000	7.3744E-07 ± 1.103E-08	1.673E+08 ± 2.146E+06	Air
MAR_11_43	-84.1082	162.0607	1744.17	1.07	0.990	0.2016	1.0482E-06 ± 1.611E-08	9.634E+07 ± 1.283E+06	Air
MAR_15_122_2	-84.1185	161.9035	1744.06	3.75	0.990	0.0731	1.3895E-07 ± 2.485E-09	7.891E+07 ± 1.271E+06	Air
MAR-11-25	-84.2087	161.3480	1837.80	1.74	0.999	0.0111	2.2807E-07 ± 1.097E-08	5.633E+07 ± 2.425E+06	MM
MAR-11-25b	-84.2087	161.3480	1837.80	1.74	0.999	0.0193	2.3889E-07 ± 2.213E-08	5.503E+07 ± 3.936E+06	MM
MAR-11-25b						0.0106	2.2388E-07 ± 1.097E-08	5.444E+07 ± 2.399E+06	MM
MAR-11-25b avg								5.473E+07 ± 3.260E+06	
MAR-11-27	-84.2085	161.3655	1836.56	1.09	0.999	0.0106	8.9096E-07 ± 3.425E-08	1.498E+08 ± 4.803E+06	MM
MAR-11-28	-84.2082	161.3619	1836.77	2.17	0.999	0.0000	5.9706E-07 ± 1.2397E-08	1.675E+08 ± 3.455E+06	Air
MAR-11-29	-84.1980	161.2660	1835.95	1.58	0.999	0.0247	2.9678E-07 ± 1.787E-08	4.544E+07 ± 2.217E+06	MM
MAR-11-29							3.1097E-07 ± 1.570E-08	4.498E+07 ± 2.062E+06	MM
MAR-11-29 avg								4.521E+07 ± 2.141E+06	MM
MAR-11-31	-84.1977	161.2584	1837.49	1.11	0.999	0.0257	2.7176E-07 ± 1.701E-08	2.463E+07 ± 1.503E+06	MM
MAR-11-31							2.2397E-07 ± 1.445E-08	3.307E+07 ± 1.702E+06	MM
MAR-11-31 avg								2.885E+07 ± 1.605E+06	
MAR-11-32	-84.1970	161.2508	1836.37	1.90	0.999	0.1144	3.8387E-08 ± 1.267E+07	1.267E+07 ± 5.055E+05	Air
MAR-11-34	-84.1971	161.2372	1836.37	1.29	0.999	0.0117	1.7393E-07 ± 9.307E-09	3.884E+07 ± 1.908E+06	MM
MAR-11-36	-84.2008	161.3194	1832.74	0.83	0.999	0.0181	3.7043E-07 ± 2.329E-08	4.271E+07 ± 2.227E+06	MM
MAR-11-36							3.8036E-07 ± 2.073E-08	4.473E+07 ± 2.255E+06	MM
MAR-11-36 avg								4.372E+07 ± 2.241E+06	
MAR-11-38	-84.2006	161.3078	1826.12	0.84	0.999	0.0925	2.3212E-07 ± 5.2394E-09	9.406E+07 ± 2.112E+06	Air
MAR-11-39	-84.2006	161.3019	1827.10	0.97	0.999	0.1158	3.7897E-07 ± 0.000E+00	1.021E+08 ± 2.255E+06	Air
MAR-11-40	-84.2006	161.3019	1827.10	2.32	0.999	0.0254	5.8912E-07 ± 2.757E-08	2.965E+07 ± 1.244E+06	MM

Notes: The samples (n=11) above the horizontal black line are from Kaplan et al. (2017).

Table 3. ^{10}Be, ^{26}Al ages from Mt. Achernar.

Sample name	^{10}Be Age ± 1σ St (yrs)	ext. err	^{10}Be Age ± 1σ Lm (yrs)	ext. err	^{10}Be Age ± 1σ LSDn (yrs)	ext. err	^{26}Al Age ± 1σ Lm (yrs)	ext. err
MAR-11-22	13800 ± 310	560	13400 ± 300	540	12100 ± 270	480	17500 ± 1380	2160
MAR-11-10	189400 ± 2880	7300	183500 ± 2790	6980	165500 ± 2500	6130	180200 ± 3610	18880
MAR-11-18	5000 ± 90	190	4800 ± 90	180	4300 ± 80	160	4900 ± 370	590
MAR-11-26	182300 ± 2690	6980	176600 ± 2600	6670	159400 ± 2340	5870	179000 ± 5120	19100
MAR-11-30	51700 ± 1220	2150	50100 ± 1190	2070	45300 ± 1070	1830	48400 ± 1150	4800
MAR-11-37	103700 ± 1350	3840	100500 ± 1300	3670	90900 ± 1180	3240	96200 ± 1950	9690
MAR-11-14a	547900 ± 6930	22390	529300 ± 6660	21240	473400 ± 5870	18300	439000 ± 10220	52600
MAR-11-14b	550700 ± 6980	22530	532100 ± 6710	21360	475800 ± 5910	18410	454600 ± 10690	54930
MAR-11-17	6300 ± 180	280	6100 ± 180	270	5600 ± 160	240	5100 ± 520	710
MAR-11-33	37500 ± 490	1370	36400 ± 480	1310	32900 ± 430	1160	31200 ± 1070	3160
MAR-15-63	82 ± 5	6	79 ± 5	5	81 ± 5	6		
MAR-15-89	15500 ± 190	560	15100 ± 180	540	13700 ± 160	470		
MAR-15-57	12500 ± 240	490	12100 ± 240	470	10900 ± 210	410		
MAR-15-58	11100 ± 210	430	10700 ± 210	410	9600 ± 190	360		
MAR-15-59	6100 ± 120	240	6000 ± 110	230	5400 ± 100	200		
MAR-15-62	4200 ± 120	190	4100 ± 120	180	3700 ± 110	160		
MAR-15-107	3400 ± 90	150	3300 ± 90	140	2900 ± 80	120		
MAR-15-108	3100 ± 90	140	3000 ± 90	130	2700 ± 80	120		
MAR-15-101	9500 ± 210	380	9200 ± 200	370	8200 ± 180	320		
MAR-15-102	14900 ± 290	580	14500 ± 280	560	13100 ± 250	500		
MAR-15-105	12300 ± 290	510	11900 ± 280	490	10700 ± 250	430		
MAR-15-110	610 ± 32	38	600 ± 31	37	520 ± 27	32		
MAR-15-123	88800 ± 1380	3360	86100 ± 1340	3220	77900 ± 1210	2850		
MAR-15-124	123800 ± 2570	5020	120000 ± 2490	4810	108400 ± 2240	4260		
MAR-15-127	19600 ± 380	770	19100 ± 360	730	17200 ± 330	650		
MAR-15-129	6100 ± 150	250	5900 ± 140	240	5400 ± 130	220		
MAR-15-130	19600 ± 370	760	19000 ± 360	730	17200 ± 320	650		
MAR-15-61	2900 ± 680	690	2800 ± 660	670	2400 ± 580	590		
MAR-15-92	8900 ± 500	590	8600 ± 490	570	7700 ± 440	500		
MAR-15-96	10100 ± 620	710	9800 ± 600	690	8800 ± 540	610		
MAR-15-113	384600 ± 7140	16010	372100 ± 6890	15250	334200 ± 6120	13300		
MAR-15-115	110100 ± 2390	4510	106800 ± 2320	4320	97000 ± 2100	3850		
MAR-15-116	109000 ± 3200	4960	105700 ± 3100	4760	96000 ± 2810	4250		
MAR-15-117	106200 ± 2540	4480	103000 ± 2470	4300	93600 ± 2230	3830		
MAR-15-118	19100 ± 650	920	18600 ± 630	880	16900 ± 570	790		
MAR-15-121	88500 ± 1710	3500	85800 ± 1660	3360	78000 ± 1500	2990		
MAR-15-64	53 ± 4	4	52 ± 4	4	54 ± 4	4		
MAR-15-65	79 ± 9	9	76 ± 8	9	78 ± 9	9		
MAR-15-111	1070 ± 25	44	1040 ± 25	42	890 ± 21	36		
MAR-15-142-T	2800 ± 60	110	2700 ± 60	110	2400 ± 50	90		
MAR-15-143	880 ± 22	37	850 ± 21	35	730 ± 18	30		
MAR-15-139	800 ± 28	39	780 ± 27	38	670 ± 23	32		
MAR-15-142-H	720 ± 29	37	700 ± 28	36	600 ± 24	31		
MAR-15-145	6400 ± 120	250	6200 ± 120	240	5600 ± 110	210		
MAR-15-132	760 ± 34	43	740 ± 33	42	640 ± 29	36		
MAR-15-133	1700 ± 80	100	1700 ± 80	90	1400 ± 70	80		
MAR-15-137	18400 ± 310	700	17800 ± 300	670	16200 ± 270	590		
MAR-15-94	9800 ± 120	350	9500 ± 120	340	8500 ± 110	300		
MAR-15-97	9300 ± 160	350	9000 ± 150	340	8000 ± 140	300		
MAR-15-87	330 ± 10	15	320 ± 10	15	290 ± 9	13		
MAR-15-88	1100 ± 20	40	1100 ± 20	40	900 ± 20	40		

Notes: External errors (ext) provided in addition to internal (analytical) errors. The samples above the horizontal black line are from Kaplan et al. (2017), and ages are recalculated as discussed in Methods.

Table 4. ^{3}He ages from Mt. Achernar.

Sample name	^{3}He Age ± 1σ St (yrs)	ext. err	^{3}He Age ± 1σ Lm (yrs)	ext. err	^{3}He Age ± 1σ LSD (yrs)	ext. err
MAR-11-08	13200 ± 1010	1770	13240 ± 1010	1770	12090 ± 920	1620
MAR-11-23	11800 ± 720	1490	11820 ± 720	1490	10770 ± 660	1360
MAR-11-52	315900 ± 7340	35510	315880 ± 7330	35510	290120 ± 6740	32620
MAR-11-48Green	108500 ± 2950	12300	108550 ± 2950	12300	99580 ± 2710	11280
MAR-11-48Red	109100 ± 3000	12370	109120 ± 3000	12370	100100 ± 2750	11350
MAR-11-21AL	23600 ± 1260	2880	23600 ± 1260	2880	21620 ± 1150	2640
MAR-11-21CM	20800 ± 1090	2530	20780 ± 1090	2530	19030 ± 1000	2320
MAR-11-35	98000 ± 2600	11090	98030 ± 2600	11090	90010 ± 2390	10190
MAR-11-01	7000 ± 630	990	7020 ± 630	990	6460 ± 570	910
MAR-11-02	7000 ± 770	1090	7040 ± 770	1090	6480 ± 700	1000
MAR-11-09	11300 ± 800	1480	11320 ± 800	1480	10300 ± 720	1340
MAR-15-112_avg	18000 ± 520	2050	18000 ± 520	2050	16470 ± 470	1870
MAR_15_120	103700 ± 1710	11530	103700 ± 1710	11530	95780 ± 1580	10650
MAR_11_41	157100 ± 2670	17490	157110 ± 2670	17490	145210 ± 2470	16160
MAR_11_42	112600 ± 1930	12540	112610 ± 1930	12540	104060 ± 1790	11590
MAR_15_126	179800 ± 3030	20010	179810 ± 3030	20010	164910 ± 2780	18350
MAR_15_119	101000 ± 1670	11240	101010 ± 1670	11240	93310 ± 1540	10380
MAR_15_125_2	135200 ± 2230	15040	135210 ± 2230	15040	123870 ± 2050	13780
MAR_15_128_2	18600 ± 370	2080	18630 ± 370	2080	17040 ± 340	1910
MAR_15_131_2	20500 ± 400	2290	20490 ± 400	2290	18750 ± 360	2090
MAR_11_13	382000 ± 6040	42450	381980 ± 6040	42450	350400 ± 5540	38940
MAR_11_15	223500 ± 3660	24860	223530 ± 3660	24860	205050 ± 3360	22800
MAR_11_43	137600 ± 2410	15330	137640 ± 2410	15330	127150 ± 2220	14160
MAR_15_122_2	115400 ± 2380	12920	115400 ± 2380	12920	106600 ± 2200	11930
MAR-11-25	74800 ± 3220	8830	74780 ± 3220	8830	68590 ± 2950	8100
MAR-11-25b	72700 ± 4330	9090	72660 ± 4330	9090	66640 ± 3970	8340
MAR-11-27	197900 ± 6350	22680	197930 ± 6350	22680	181680 ± 5830	20820
MAR-11-28	212700 ± 6680	24340	212730 ± 6680	24340	195270 ± 6130	22340
MAR-11-29	60000 ± 2840	7190	60020 ± 2840	7190	55040 ± 2610	6590
MAR-11-31	38100 ± 2120	4700	38100 ± 2120	4700	34900 ± 1940	4300
MAR-11-32	14300 ± 1530	2190	14270 ± 1530	2190	13020 ± 1400	2000
MAR-11-34	51400 ± 2530	6190	51420 ± 2530	6190	47140 ± 2320	5680
MAR-11-36	57800 ± 2960	7010	57800 ± 2960	7010	53010 ± 2720	6430
MAR-11-38	108700 ± 4220	12680	108660 ± 4220	12680	99780 ± 3880	11640
MAR-11-39	118100 ± 4360	13700	118080 ± 4360	13700	108430 ± 4000	12580
MAR-11-40	39900 ± 1670	4690	39870 ± 1670	4690	36560 ± 1530	4310

Notes: External errors (ext) provided in addition to internal (analytical) errors. The samples above the horizontal black line are from Kaplan et al. (2017), and ages are recalculated as discussed in Methods. For samples measured twice, on figures we show an average age and the higher of the two respective errors.

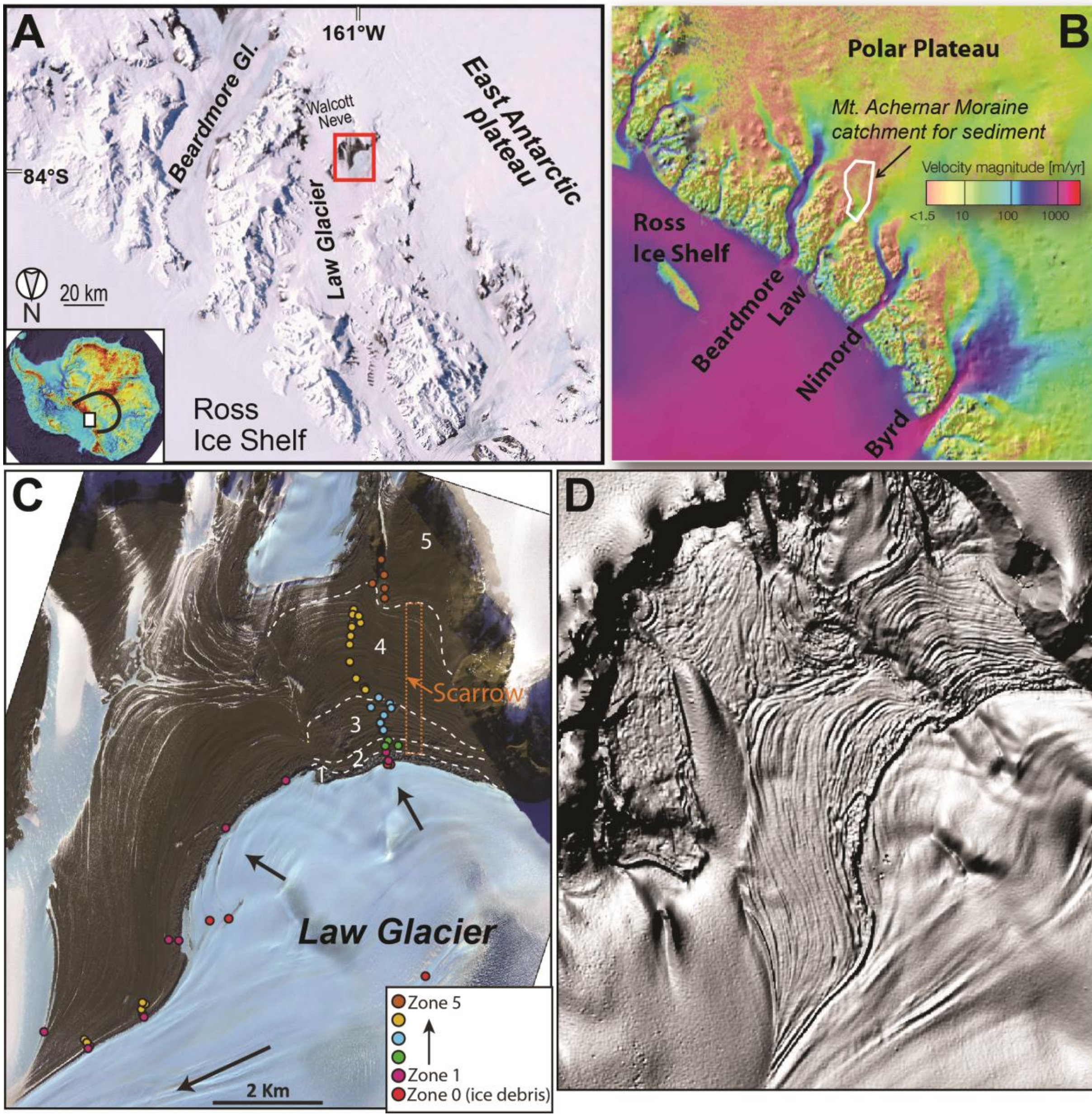

Figure 1. Setting of the Mt. Achernar area. A) Mt. Achernar moraine sits at the head of Law Glacier (within red box) where unconstrained flow off of the East Antarctic plateau becomes constrained through Transantarctic Mountains. B) Ice surface velocities and sediment catchment area for the Mt. Achernar area (Bader et al. 2017; Graly et al., 2018b). C) The entire moraine complex along with locations of sediment (till) samples for study of provenance changes (Bader et al., 2017) and soil geochemistry (Graly et al., 2017). Also shown are zones (in white) defined in Bader et al. (2017), the general area of study by Scarrow et al. (2014), and ice flow directions with arrows. Note the ice flow is steered away from the main trunk glacier, where it is then trapped in the embayment (Kassab et al. 2020). D) Image of the Achernar moraine and surrounding area, from Antarctic REMA (Reference Elevation Model of Antarctica) Explorer (Howat et al., 2019).

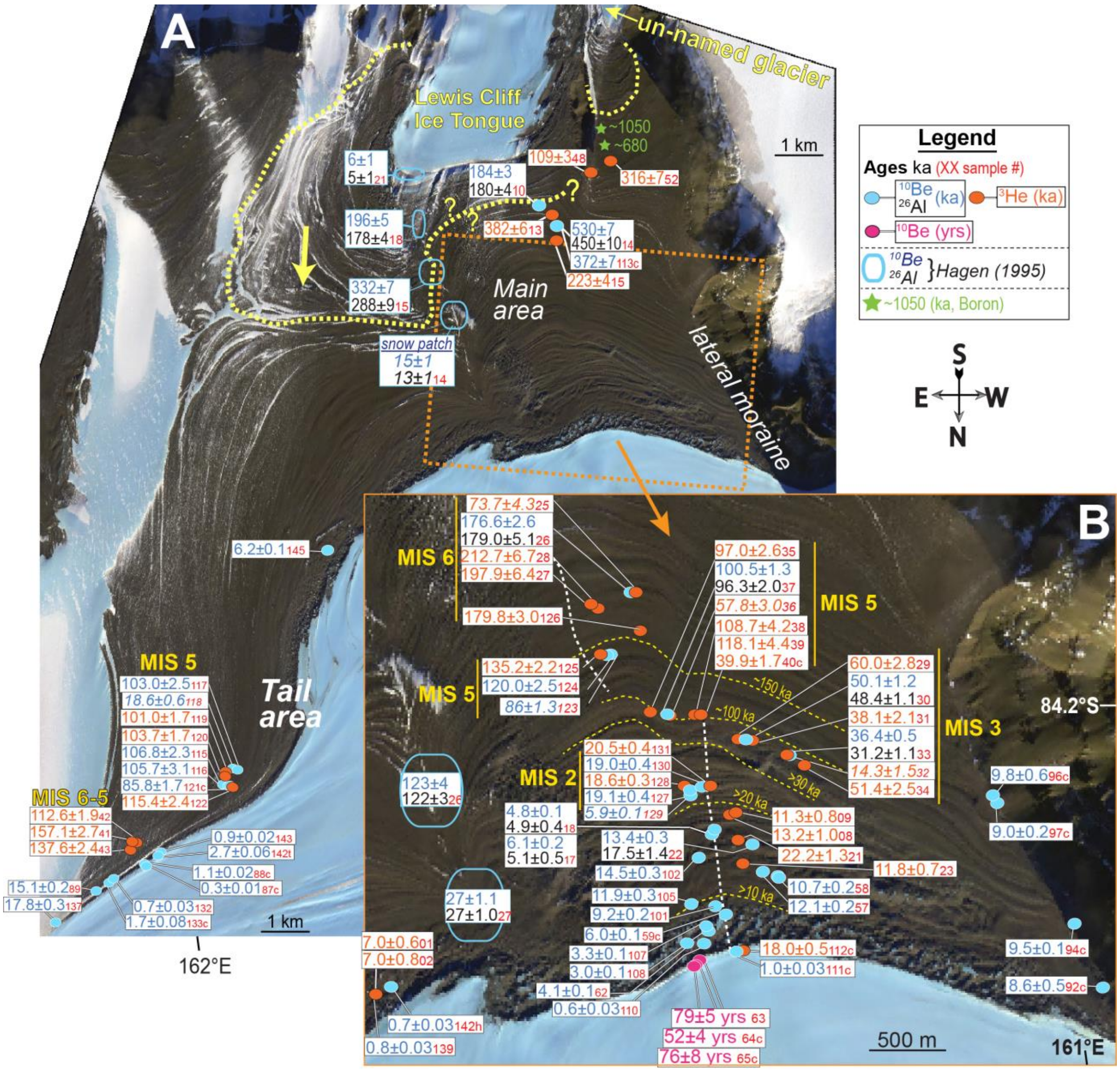

Figure 2. All ^{10}Be-^{26}Al-^{3}He ages obtained in the Mt. Achernar area. A) The study area including the tail area (NW sector), which is shown in more detail in Figure 5. The yellow-dashed line outlines moraine associated with the Lewis Cliffs Ice Tongue, which impinged on and disturbed the Mt. Achernar blue-ice moraine. We show the two oldest boron-exposure ages (Graly et al., 2018a) (Fig. 1C), in the southwestern sector, to the right of Lewis Cliffs Ice Tongue. B) A focus on the main and lateral moraine areas, which are shown in more detail in Figures 3 and 4. Italicized ages are discussed as outliers. All exposure ages are on boulders except those labelled 'c' (cobble-size). All ages in ka, except for three 10Be ages in pink (years), which are on samples from the Law Glacier margin (see next, Figure 3 for more detail). Yellow-dashed lines with associated ages mark approximate age boundaries.

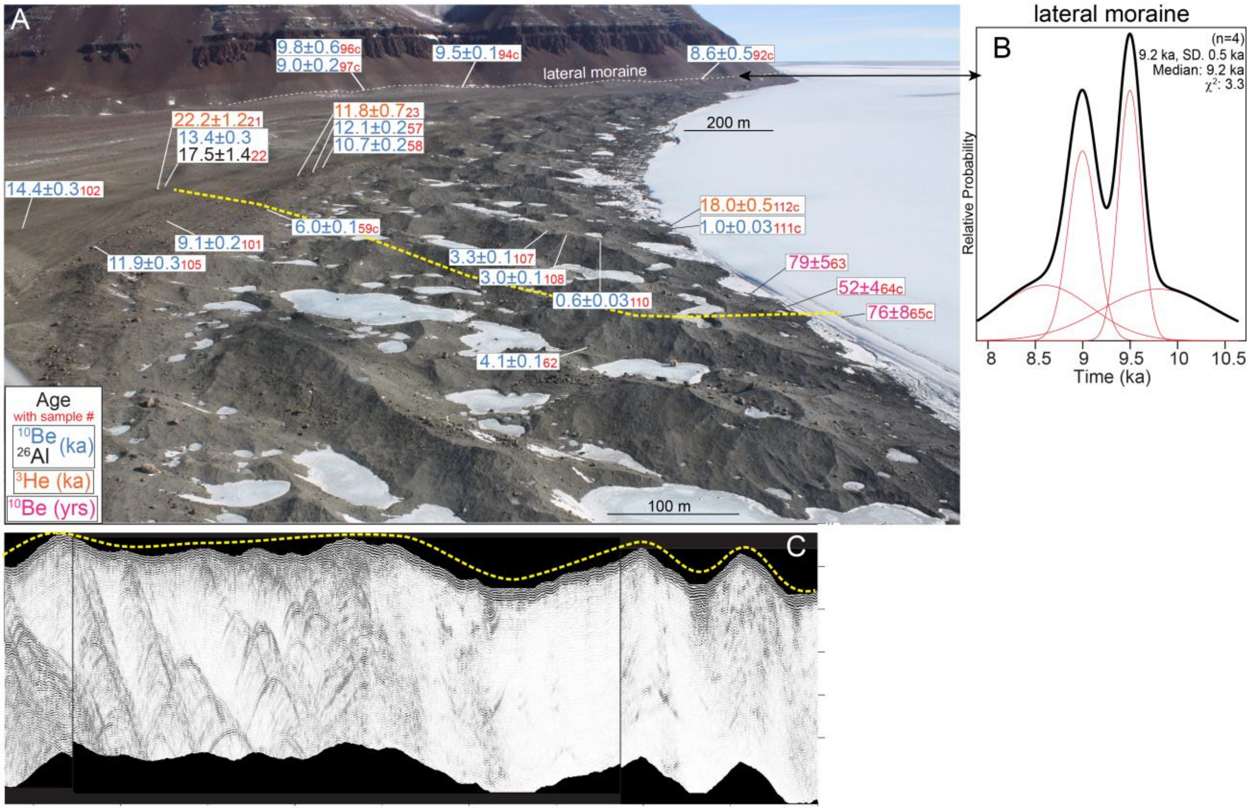

Figure 3. Focus on the best-dated Zones 1 and 2, looking west with the Law Glacier on the right. Headwall of Mt. Achernar shown in background. Four ^{10}Be ages on samples along the lateral moraine, date to 9.2 ± 0.5 ka and record a high surface for ice flowing off the plateau, which is seen in the upper right. GPR radargram profile below the photo is from Kassab et al. (2020), and more or less follows the yellow-dashed line. Dipping stacked and scatterred hyperbolas are inferred to represent planes of debris and cobbles/boulders causing point reflectors, respectively. Figure 6 provides additional photos of the lateral moraine with samples.

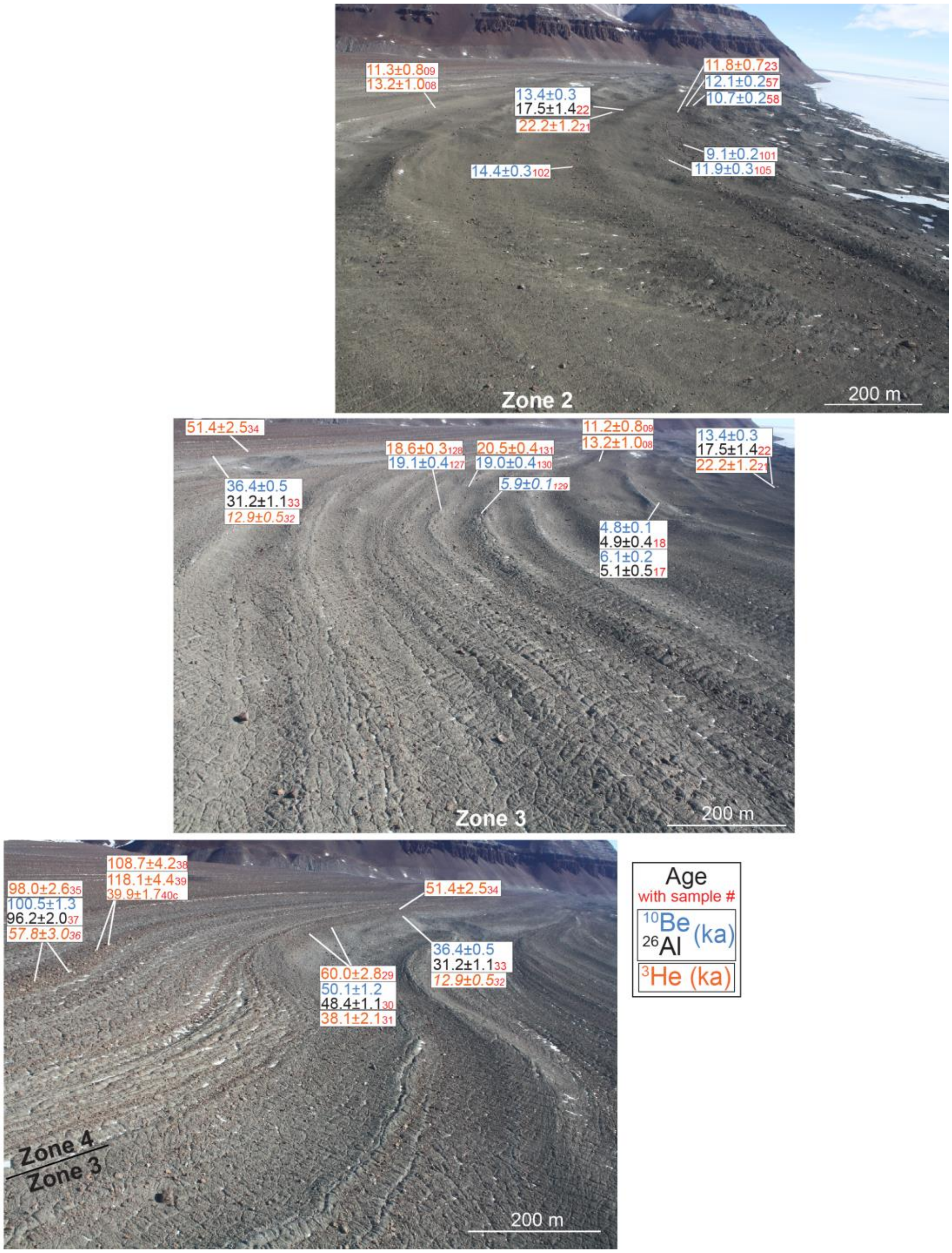

Figure 4. Similar to Figure 3, with photos focusing on Zones 2 to 4 and cosmogenic exposure ages. Top panel focuses on Zone 2, with the Law Glacier (Fig. 3) on right side. Middle panel focuses on Zones 2 and 3 including moraines dated to MIS 2 time; the average and standard deviation are 19.3±0.8 ka excluding the one outlier of 5.9±0.1. Bottom panel focuses on inner Zone 4 and samples dating to <100 ka. Mt Achernar headwall is in the background. In each subsequent panel, some overlap in exposure ages is shown on right side.

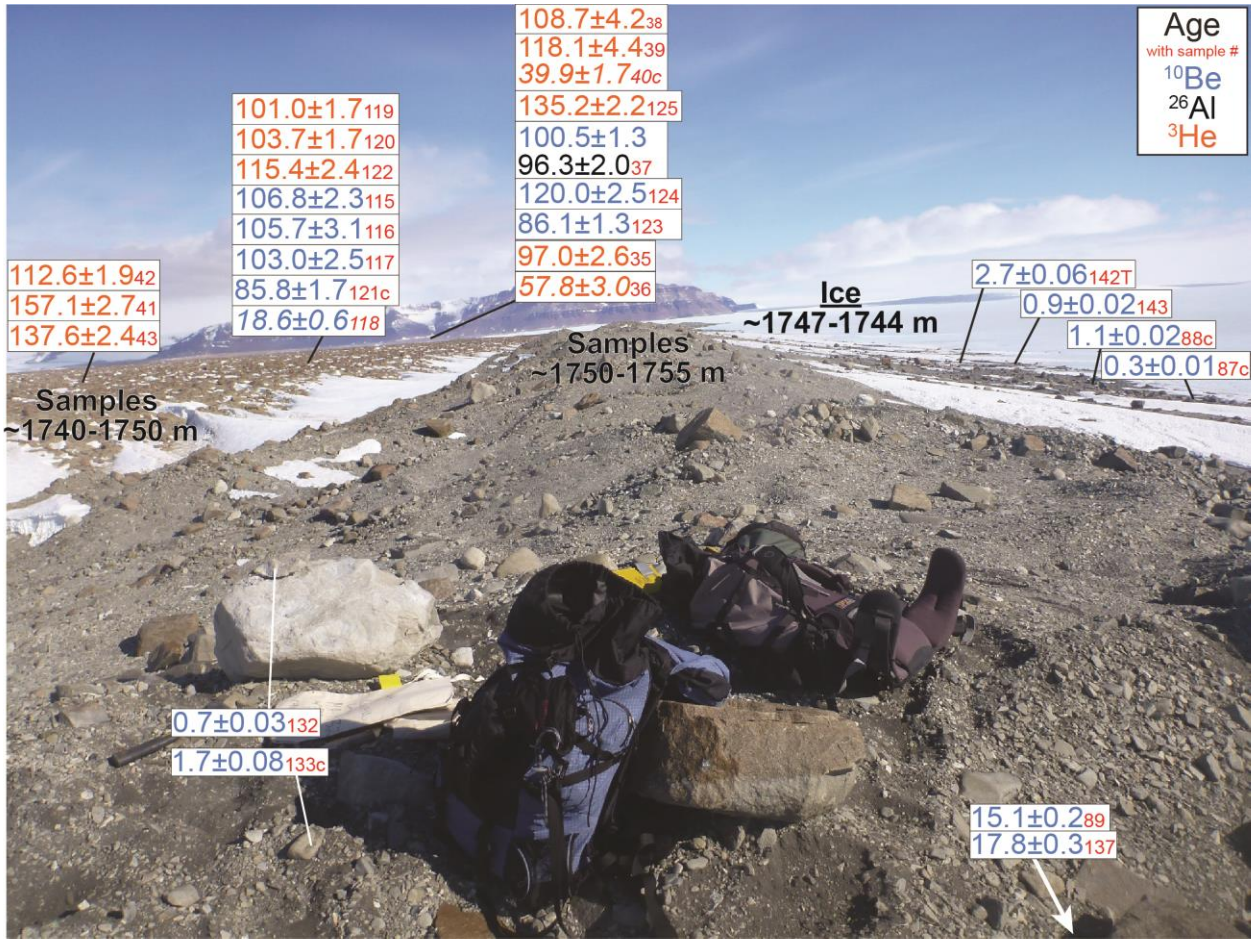

Figure 5. A focus on the tail area, with view looking southwest, towards Mt. Achernar. Law Glacier is on the right. Note relatively oxidized sediments on the left side of the photo, which date to MIS 6 and 5 except for 1 outlier of ~18.6 ka. Also shown are MIS 5 ages (~135.2 to ~86.1 ka) from the main area of focus (Fig. 2B), which is in the background. All are boulder ages except if labelled "c" (cobble size). Two outliers are italicized. See Figure 6 for photos that focus on the right side of image; both the ~0.3 and ~0.9 ka ages are slightly closer to the present margin, compared with the ~1.1 and ~2.7 ka ages.

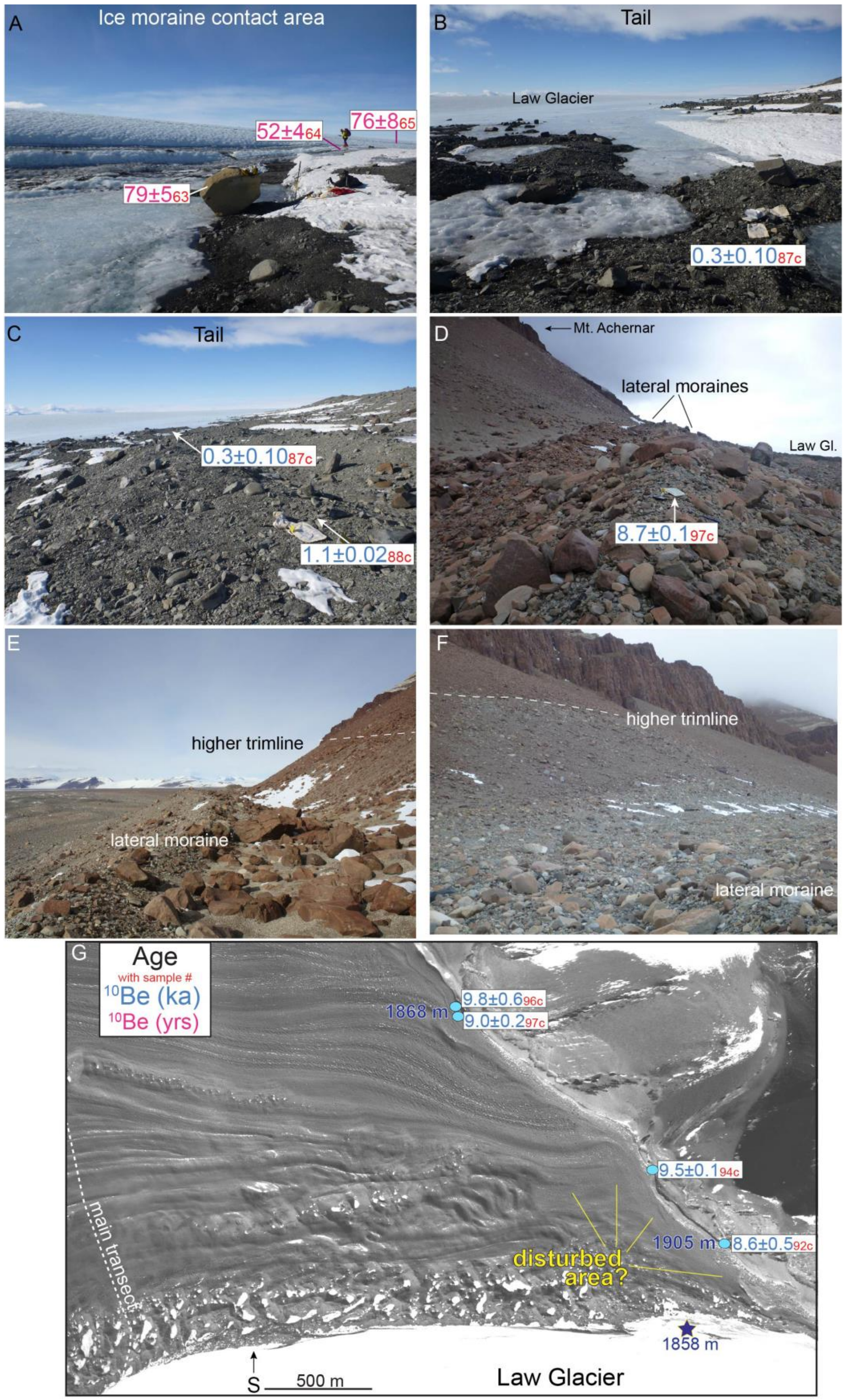
A
Ice moraine contact area
52±4 64
76±8 65
79±5 63
B
Tail
Law Glacier
0.3±0.10 87c
C
Tail
0.3±0.10 87c
1.1±0.02 88c
D
Mt. Achernar
lateral moraines
Law Gl.
8.7±0.1 97c
E
higher trimline
lateral moraine
F
higher trimline
lateral moraine
G
Age
with sample #
10Be (ka)
10Be (yrs)
1868 m
9.8±0.6 96c
9.0±0.2 97c
9.5±0.1 94c
1905 m
8.6±0.5 92c
disturbed
area?
main transect
1858 m
S
500 m
Law Glacier

Figure 6. Photos that provide context of geomorphology and age data. A) Three 10Be ages near the moraine/ Law Glacier boundary. Person for scale. In this panel the three ages are in years, in all other panels they are in ka. B) and C) A focus on the tail area and samples MAR-15-87 (ice margin) and -88 (+4 m). D) The lateral moraine, with two apparent ridges. E) The lateral moraine and trimline, close to (NW of) sample MAR-15-92c (panel G). The tallest boulders are ~1 m in height and we estimate the trimline is about 15-20 m higher. F) The lateral moraine and trimline, by MAR-15-98c (panel G). We estimate the trimline is <10 m higher. G) The area near the lateral moraine with ^{10}Be ages (all cobbles). We also show the elevation difference between the Law Glacier (1858 m), lateral moraine (~1905 m), and towards the south (1868 m). Note the area next to the lateral moraine is smoother without distinct ridges, as exists to the left (east) closer to the area of the main transect (white-dashed line, Fig. 2). We infer disturbances within ~500 m of the lateral moraine due to the rise in surface by ~10-9 ka and when the trimline formed.

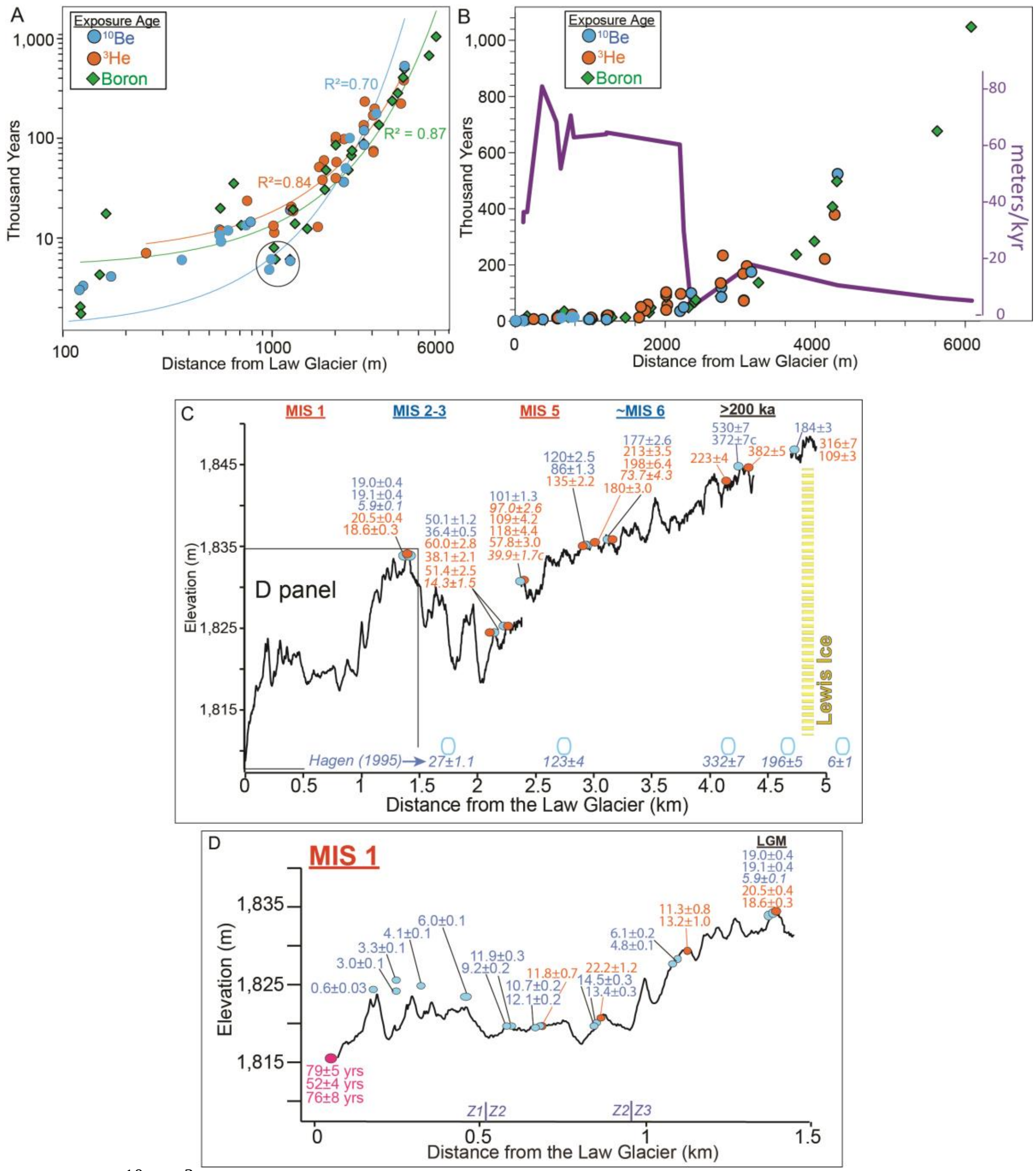

Figure 7. ^{10}Be-^{3}He-Boron exposure ages with distance from the Law Glacier along the main transect (white-dashed line, Fig. 2). **Panels A, B**) Left side is plotted as log-log plot. Three respective exponential relations demonstrate there is a steady increase in age from the active margin. Within ~2200 m (~50 ka) from the Law Glacier, if the relation is represented by a linear line, the r^2 is ~0.8 (^{10}Be) or ~0.6 (^{3}He). Boron ages are from Graly et al. (2018a). Circle marks younger sediment dated, where ^{10}Be-^{26}Al-Boron exposure ages all indicate exposure for less time. In panel B, approximate average accretion rate based on ^{10}Be and the two oldest Boron ages at ~5600-6100 m. **Panels C, D)** Topographic profiles from Bader et al. (2017) and Kaplan et al. (2017). In panel C, the ages from Hagen (1995) are at the bottom because it is not clear how they align with the main transect. MIS labels are approximately located with distance. For simplicity, ^{26}Al ages are not shown. In Panel D, Zones 1 to 3 (Z1-Z3) are shown along bottom.

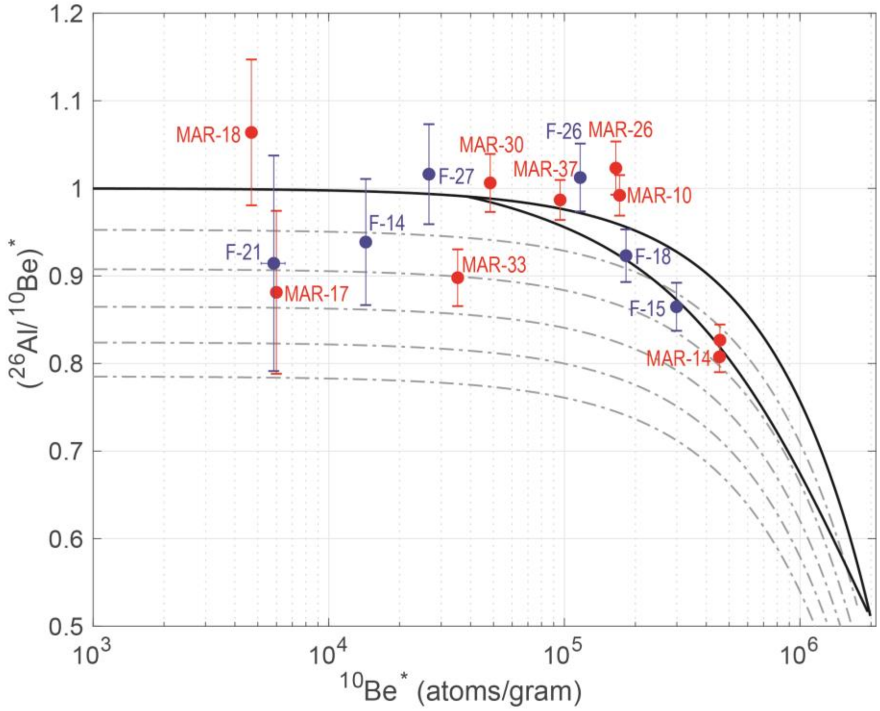

Figure 8. Plot of $^{26}Al/^{10}Be$ ratios versus ^{10}Be concentrations, with data colored in blue and red from Hagen (1995) and Kaplan et al. (2017), respectively, recalculated with updated systematics. MAR-11-22 is not shown on the plot due to its high $^{26}Al/^{10}Be$ value (Table 1). The first and last parts of each sample name are shown next to analyses. The ratios are standardized (*) to 6.75, the Be-10 concentrations are relative to 07KNSTD and sea level high latitude (Balco et al., 2008). Error bars are 1σ analytical uncertainty.

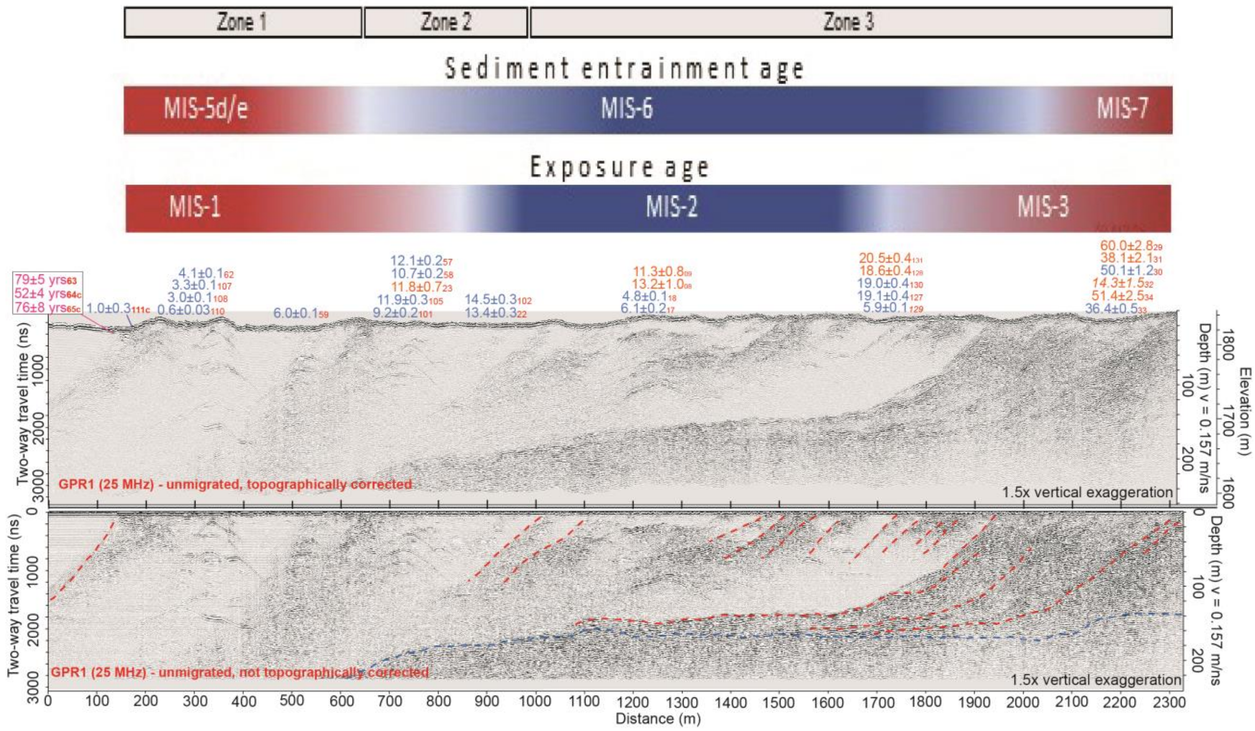

Figure 9. Ground Penetrating radar (GPR, 25MHz) with approximate locations of ^{10}Be-^{3}He above the topographically corrected surface. Ages are shifted slightly so as to be at their approximate location along GPR transect. The upper panel is the processed radargram and the lower panel has interpretations including red-dashed lines as debris planes. Kassab et al. (2020) interpreted the blue-dashed line, which represents a continuous subhorizontal reflector, to be the bedrock surface at ~140 m to >220 m below. Above the GPR data, we show both maximum sediment entrainment age (Graly et al., 2020, Kassab et al. 2020) and surface exposure ages. Boundaries between MIS are fuzzy given ranges of ages. Kassab et al. (2020) also presented GPR analyses for inner Zone 4, with exposure ages ≥100ka, but they found a lack of consistent GPR reflections. For simplicity, ^{26}Al ages are not shown.

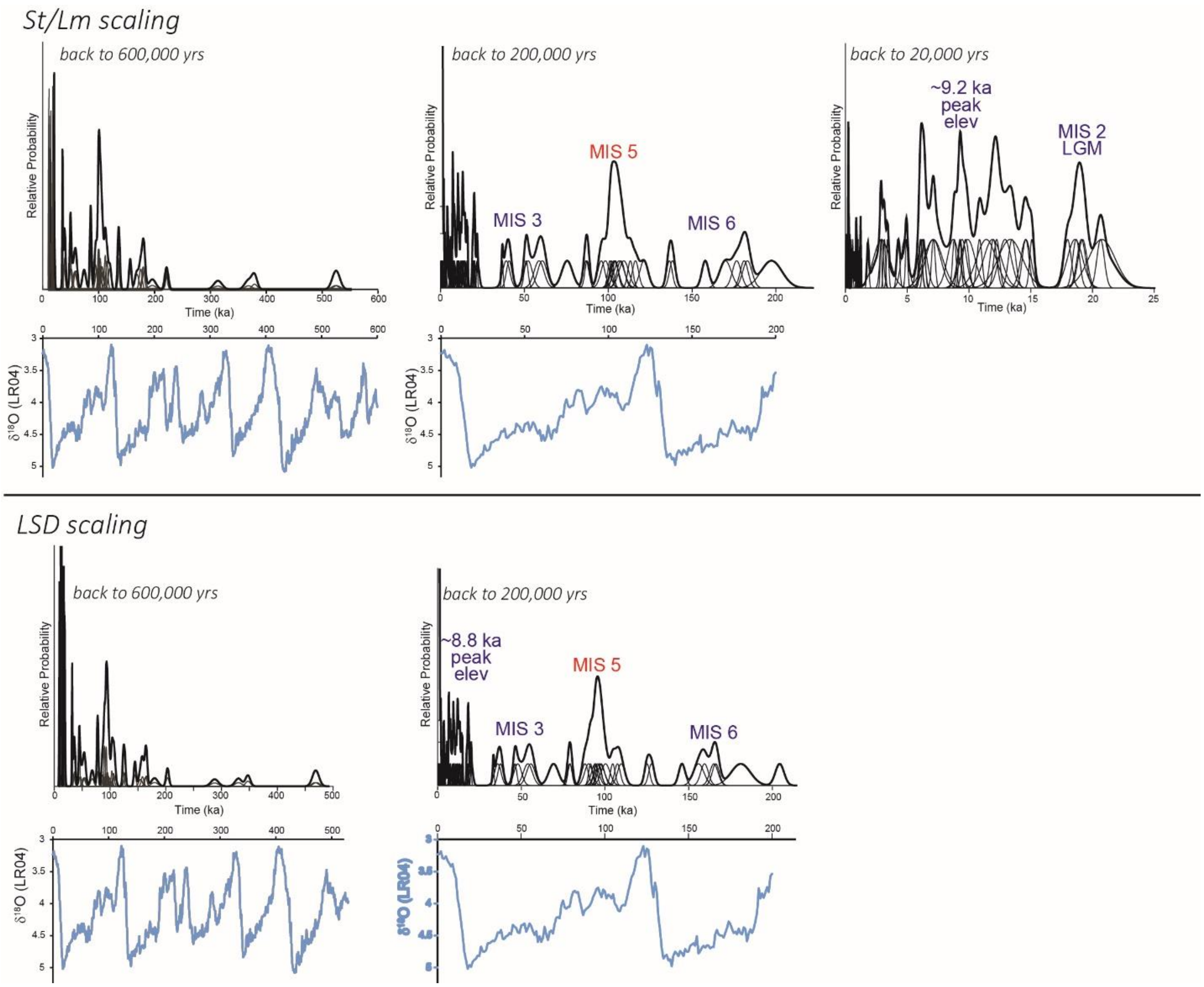

Figure 10. ^{10}Be-^{26}Al-^{3}He ages compared with benthic δ^{18}O stack (Lisiecki and Raymo, 2004). Top panels include ages with St/Lm scaling (difference not discernable at the scale shown). During MIS 5, a concentration of ages occurs at 120-100 ka excluding "outlier' ages <90 ka from the same sites (Fig. 5). Taken at face value these ages overlap with MIS5c or 5c-d. Bottom panels include exposure ages calculated with the LSDn scaling (Table 1,3) method, which are ~10-12% lower than those calculated using St/Lm.